Combining airborne thermal infrared images and radium isotopes to study submarine groundwater discharge along the French Mediterranean coastline

Simon Bejannin, Pieter Van Beek, Thomas Stieglitz, Marc Souhaut, Joseph Tamborski

Journal of Hydrology: Regional Studies 13 (2017) 72–90

Contents lists available at ScienceDirect

Journal of Hydrology: Regional Studies

journal homepage: www.elsevier.com/locate/ejrh

Combining airborne thermal infrared images and radium isotopes to study submarine groundwater discharge along the French Mediterranean coastline

Simon Bejannin[a,*], Pieter van Beek[a], Thomas Stieglitz[b,c], Marc Souhaut[a], Joseph Tamborski[a]

[a] LEGOS, Laboratoire d'Etudes en Géophysique et Océanographie Spatiales (CNRS/UPS/CNES/IRD),Observatoire Midi-Pyrénées14 Avenue Edouard Belin, 31400 Toulouse, France

[b] CEREGE, Centre de Recherche et d'Enseignement de Géosciences de l'Environnement (Aix Marseille Univ, CNRS, IRD, Coll France), 13545 Aix-en-Provence, France

[c] Centre for Tropical Water & Aquatic Ecosystem Research and School of Engineering & Physical Sciences, James Cook University, Townsville, QLD 4811, Australia

ARTICLE INFO

Keywords:
Submarine groundwater discharge
Mediterranean sea
Radium isotopes
Thermal infrared remote sensing
Fluxes
GEOTRACES

ABSTRACT

Study region: The French Mediterranean coastline, which includes karstic springs discharging into coastal seas and coastal lagoons.

Study focus: We investigated submarine groundwater discharge (SGD), an important vector for many chemical elements that may impact the quality of the coastal environment. First, we acquired airborne thermal infrared (TIR) images to detect terrestrial groundwater inputs. Then we report *in situ* data (salinity; temperature; radium isotopes). We use these data i) to confirm the presence of groundwater discharge and to characterize the different systems, and ii) to quantify SGD fluxes and estimate the residence time of the water bodies.

New hydrological insights for the region: Few studies have been conducted on SGD along the French Mediterranean coastline. The terrestrial groundwater spring inputs in La Palme and Salses-Leucate coastal lagoons are in the range (0.04–0.11) $m^3 s^{-1}$, ≤ 2% of the local river inputs. In comparison, total SGD estimates to La Palme lagoon (0.56–1.7 $m^3 s^{-1}$) suggest that the recirculation of lagoon water through the sediment is two orders of magnitude greater than the terrestrial groundwater inputs. At the Calanque of Port-Miou, the terrestrial groundwater flux to the coastal seas was between 0.6 and 1.2 $m^3 s^{-1}$ in July 2009. This study demonstrates the application of airborne TIR remote sensing for detecting surficial groundwater springs, and the inability of the method to detect deeper, submerged springs.

1. Introduction

Submarine groundwater discharge (SGD) is recognized as an important pathway at the continent-ocean interface for the transfer of chemical elements and species into coastal waters. Global estimates of terrestrial SGD vary between 0.2–10% of the global river flow (COSOD II, 1987; Taniguchi et al., 2002), therefore, SGD can be both volumetrically and chemically important to coastal waters (Slomp and Van Cappellen, 2004). This input term may have a significant impact on the quality of the coastal waters and ecosystems,

* Corresponding author at: 14 Avenue Edouard Belin, 31400 Toulouse, France.
E-mail address: simon.bejannin@legos.obs-mip.fr (S. Bejannin).

http://dx.doi.org/10.1016/j.ejrh.2017.08.001
Received 27 February 2017; Received in revised form 21 July 2017; Accepted 2 August 2017
Available online 22 August 2017

as well as on geochemical cycles. In its commonly used definition, SGD includes both i) the discharge of terrestrial (i.e. fresh) groundwater driven by a positive hydraulic gradient between the coastal aquifer and the sea and ii) seawater recirculation through permeable sediments driven by physical processes, such as waves and tides (Burnett et al., 2006). The mixing zone between groundwater and seawater within the coastal aquifer is defined as the subterranean estuary, where many chemical reactions take place, thus releasing or removing chemical species into coastal waters (Moore, 1999). Several studies have concluded that SGD has a significant impact on oceanic biogeochemical cycles, such as radium (Kwon et al., 2014; Moore, 2008; Rodellas et al., 2015), rare earth elements (Johannesson and Burdige, 2007), nutrients (Beusen et al., 2013; Slomp and Van Cappellen, 2004) and mercury (Bone et al., 2007).

Among the methods employed to study SGD, airborne thermal infrared (TIR) remote sensing can be used to detect cold or warm groundwater inputs into coastal seas because of the thermal contrast between groundwater and the surrounding coastal waters. This technique has been used in various places of the world, and is effective because of its combined use with *in-situ* measurements, including salinity and geochemical tracers such as radon and radium (Kelly et al., 2013; Lee et al., 2009; Mejías et al., 2012; Mulligan and Charette, 2009; Tamborski et al., 2015; Wilson and Rocha, 2012). Radon and radium isotopes are powerful tools to quantify SGD fluxes as they are enriched in groundwater relative to coastal waters. Ra is produced in the aquifer by the decay of Th on or near the sediment grain surface. Ra is particle-reactive and is adsorbed onto the surfaces of sediments at low ionic strengths (i.e. freshwater), but is released into solution upon contact with higher ionic strength (i.e. saline) waters, making Ra isotopes useful tracers of SGD (Swarzenski, 2007; Charette et al., 2008). The radium quartet's wide-range of half-lives (^{224}Ra, 3.66 d; ^{223}Ra, 11.4 d; ^{228}Ra, 5.75 y; ^{226}Ra, 1600 y) can be used to quantify SGD fluxes on different time-scales (Moore, 1996; Charette et al., 2001).

Although SGD has been investigated in many places of the world (Charette et al., 2001; Burnett et al., 2007; Moore, 2006; Stieglitz, 2005), including the Mediterranean Sea (Garcia-Solsona et al., 2010; Rodellas et al., 2015; Trezzi et al., 2016), very few studies have been conducted along the French Mediterranean coastline, despite the presence of several well-known karstic springs. The magnitude of SGD and its relative importance in chemical budgets of the Mediterranean Sea, and specifically the French Mediterranean, are unknown. Several karstic springs are indeed known to discharge into coastal seas or into coastal lagoons along the French Mediterranean coastline, including the submarine springs of Port-Miou and Cassis located in Calanques of Marseille-Cassis (Arfib and Charlier, 2016), Vise spring in Thau Lagoon (Condomines et al., 2012; Elbaz-Poulichet et al., 2002), Font Estramar and Font Dame springs that are connected to Salses-Leucate Lagoon (Fleury et al., 2007) and springs in La Palme lagoon (Wilke and Boutiere, 2000; Fleury et al., 2007; Stieglitz et al., 2013).

To our knowledge, Lévêque et al. (1972) conducted the first TIR survey along the French coastline, along the south-western Atlantic coast. Stieglitz et al. (2013) published a TIR image acquired in La Palme lagoon; this image comes from the same airborne survey used in this study. Schubert et al. (2014) used Landsat images of sea surface temperature anomalies from the bay of Roquebrune (southern France) to investigate a submarine spring (Cabbé). Few studies have been conducted on SGD along the French Mediterranean coastline using Ra and Rn as geochemical tracers: Ollivier et al. (2008) measured radium isotopes in the Gulf of Lions to estimate a SGD flux that was 1.6–29% of the regional river flow, Condomines et al. (2012) studied the thermal waters of Balaruc-les-Bains on the Mediterranean coast and Stieglitz et al. (2013) studied SGD in several coastal lagoons using radon as a tracer. Stieglitz et al. (2013) thus quantified groundwater discharge and seawater recirculation in La Palme lagoon, where the discharge of low-salinity karstic groundwater was found to maintain a brackish ecosystem functioning throughout the dry summer months, while wind-driven seawater circulation contributed up to 50% of the total radon fluxes to the lagoon.

Airborne thermal infrared images as well as radium isotopes have been widely used to detect and/or quantify SGD all over the world. Despite the presence of many well-known springs along the French Mediterranean coastline, these methods have hardly ever been used in this region. The aim of the present study is thus to apply thermal imagery and radium to provide information on SGD fluxes along the French Mediterranean coastline. Here, we report airborne TIR images that were acquired along the French Mediterranean coastline. To complement the TIR images, we collected *in situ* data (salinity, temperature, radium isotopes) to characterize the different sites and to provide quantitative information (SGD fluxes, residence times of surface waters) regarding the different systems.

2. Material and methods

2.1. Study sites

In this study, we report data obtained throughout four different regions along the French Mediterranean coastline where groundwater discharge is known to take place (Fleury et al., 2007). The four investigated areas include coastal seas and coastal lagoons (Fig. 1). For many of these locations, there are known groundwater-fed karstic springs that connect to the adjacent water body *via* a small stream. We follow Stieglitz et al. (2013) in defining these systems as groundwater discharge. In this manuscript, we categorize SGD into two categories: terrestrial groundwater and marine groundwater. Terrestrial groundwater includes all flow derived from meteoric water (precipitation) coming from springs driven by a positive terrestrial hydraulic gradient. We keep the terminology "terrestrial groundwater" despite the salinity (2–10) of the discharging water at the spring outlets because these waters have a terrestrial origin. On the other hand, marine groundwater includes seawater (and lagoon water) recirculation through permeable coastal sediments, which subsequently flows back to the sea (and lagoon) with a different chemical composition. Marine SGD is driven by various physical forcing mechanisms, and is distinct from water fluxes driven by pore water exchange and bioturbation (Santos et al., 2012). The four investigated areas are described below (Fig. 1):

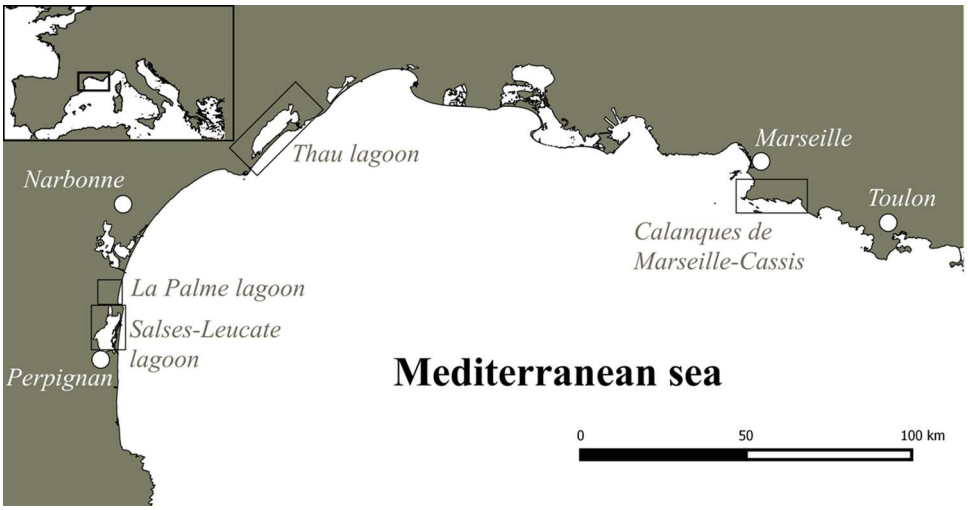

Fig 1. Location of the different sites investigated in this study along the French Mediterranean coastline.

2.1.1. La Palme lagoon

La Palme lagoon (ca. 500 ha) is located south of the city Narbonne and north of Salses-Leucate lagoon which is larger in size. It is characterized by terrestrial groundwater inputs associated with karstic springs that are connected to the lagoon. La Palme lagoon is very shallow (depth between 0.2 and 1.7 m) and is connected to the sea by a small outlet that may be seasonally closed (i.e. summer time).

2.1.2. Salses-Leucate lagoon

Salses-Leucate lagoon is located on the French Mediterranean coast, north of Perpignan and south of Narbonne. The lagoon (~5400 ha) is a shallow basin with a mean depth of 2 m for the northern part and 1 m for the southern part. The salinity of the lagoon ranges between 20 and 30, and is connected to the sea by three narrow openings. The Salses-Leucate lagoon ecosystem is of notable interest related to economic activities including shellfish production, tourism and industry. Terrestrial groundwater inputs associated with karstic springs (Font Estramar and Font Dame springs) are notable in the south-west region of the lagoon. The Font Estramar spring is the main outlet of the karst formation of the eastern Corbières and covers a surface area of ~200 km^2 (Fleury et al., 2007). The Font Dame spring originates from the middle of a large swamp and is composed of water from several nearby springs with different salinities. The Font Dame spring is also an outlet of the karst formation of the eastern Corbières.

2.1.3. Calanques of Marseille-Cassis

The spring of Port-Miou flows in the Calanque of Port-Miou, east of Marseille at 12 m below sea level, from a large conduit of ~100 m^2. Seawater intrusion takes place upstream, thus raising the salinity of the groundwater that flows at the outlet (Arfib et al., 2006). A dam was constructed to prevent seawater intrusion, which has resulted in surface water salinities less than 6. Several other springs are located in the Calanque of Port-Miou (Gilli, 2001). Further east, the Bestouan spring is located at the entrance of Cassis harbor. This spring is a gallery with a smaller conduit of 10–15 m^2. The depth of this spring reaches 27 m below sea level at 400 m distance from the outlet (Cavalera, 2007).

2.1.4. Thau lagoon

Thau lagoon (7500 ha, mean depth 4 m) is one of the largest lagoons located on the French Mediterranean coast, with a drainage basin that covers approximately 280 km^2. The lagoon is fed by seawater mainly through the Canal of Sète. In addition, it receives minor quantities of terrestrial groundwater through the Vise karstic spring, while discharge varies according to the season, sewage treatment plant discharge and the Vene River (Elbaz-Poulichet et al., 2002). The Vise spring discharges at 30 m depth with a salinity less than 5 (Fleury et al., 2007). The water of the spring is composed of three endmembers, including a shallow karstic aquifer, a deep thermal circulation and seawater which proportions vary with hydrological conditions (Aquilina et al., 2002). During dry periods, the Vise spring is prone to salt water intrusion from the lagoon (this event is known as “inversac”).

2.2. Thermal infrared images (TIR)

TIR images were acquired along the French Mediterranean coastline on 20 September 2012 using a FLIR Systems ThermaCAM SC 3000. The flight and acquisition of the airborne TIR images were funded by CNES (French space agency) and were operated by TCC company (Beauvais, JC Barré). The flight was conducted at 800 m altitude during a day without wind and small waves. September was chosen to provide the largest temperature difference, where the thermal contrast between groundwater and the surrounding seawater or lagoon water would be greatest. The outward flight was made in the morning (from 7:00 am to 10:00 am) between

Toulon and Perpignan (Fig. 1) whereas the return flight was made at the end of the afternoon (4:00 p.m. to 6:30 p.m.). The TIR camera has a wave-length ranging from 8 to 12 μm with 4096 grey levels set on a temperature palette between −10 to 30 °C, with a thermal accuracy of ± 1 °C. The camera has a 1.1 mrad instantaneous field of view; at 800 m altitude, the pixel field of view is approximately 0.88 m. The TIR camera has an automatic atmospheric transmission correction based on the atmospheric temperature, relative humidity and object distance. Pixel radiance was converted into kinetic temperature assuming a constant emissivity value of water using Planck's law (1.00). Absolute temperature changes can be caused by solar heating, evaporation cooling, reflected radiance or surface water roughness; however, these will not influence the data interpretation, as SGD studies depend upon relative temperature differences (Kelly et al., 2013; Tamborski et al., 2015). However, two automated sensors (Schlumberger Water Services) were placed *in situ* in La Palme lagoon to record the water temperature with an accuracy of ± 0.1 °C at the same time as the airborne TIR image acquisition. The sensors were attached onto a buoy floating in surface waters to make sure that they recorded the surface temperature. Despite these efforts, there may be differences between the temperature derived from the airborne TIR image (top 100 μm of the water column) and that derived from the *in situ* sensors (upper few cm of the water column). TIR images were cropped and overlain on visible-light orthorectified imagery (Google Earth) to improve visualization.

2.3. Radium activities

2.3.1. Sample collection

Surface water samples (20 L) were collected using either a submersible pump or a manual pump in the different regions described above to analyze Ra isotopes. The samples were collected in Calanque of Port-Miou on 7 July 2009, in Thau lagoon (Vise spring) on 21 July 2009, in Salses-Leucate lagoon (Font Estramar and Font Dame springs) on 12 April 2016 and in La Palme lagoon on 13 April 2016. For La Palme lagoon, we also report surface water data acquired in July 2009. The springs were sampled by placing the pump closest toward the vent. For each groundwater-fed spring, water samples were collected along the stream and/or Calanque that carries the groundwater into the adjacent water body. Salinity was recorded *in situ* during the sampling operations using a WTW probe (Xylem). The 20 L water samples were passed through MnO_2-coated acrylic fibers ("Mn-fiber"), at a flow rate less than 1 L min^{-1} to ensure a 100% yield of radium extraction (Moore and Reid, 1973). Once back in the laboratory, the fibers were rinsed three times with Ra-free deionized water and dried with compressed air until a water:fiber ratio of 1:1 was reached (Sun and Torgersen, 1998).

2.3.2. Analysis of radium isotopes

Short-lived ^{223}Ra and ^{224}Ra activities were determined using a Radium Delayed Coincidence Counter (RaDeCC; Moore and Arnold (1996)). We applied the method and corrections described by Moore (2008) and Garcia-Solsona et al. (2008a) to determine detector efficiencies and propagate counting uncertainties. Four counting sessions were necessary to determine both excess ^{223}Ra and ^{224}Ra activities (denoted $^{223}Ra_{ex}$ and $^{224}Ra_{ex}$). A first session was run after sample collection to determine the total ^{224}Ra and ^{223}Ra activities. In case of high ^{224}Ra activities in the samples, another session was run after one week to determine the total ^{223}Ra activity. The Mn-fibers were analyzed again 3 weeks after sampling to determine the ^{224}Ra activities supported by ^{228}Th and then after 3 months to determine the ^{223}Ra activities supported by ^{227}Ac (Moore, 2000). The Ra activities were thus corrected for their supported activities to provide excess Ra activities. It is these excess Ra activities that are discussed in the paper.

The long-lived isotopes ^{226}Ra and ^{228}Ra were determined using the low-background gamma detectors at the LAFARA underground laboratory in Ferrières, French Pyrénées (van Beek et al., 2010, 2013). Prior to analysis, the Mn-fibers were dried, pressed using a hydraulic press at 50 metric tons and placed into plastic boxes. These boxes were then placed in plastic bags and sealed under vacuum to avoid any ^{222}Rn loss. The samples were analyzed after 3 weeks to ensure secular equilibrium between ^{226}Ra and its daughters using a semi-planar detector (ORTEC/AMETEK; van Beek et al., 2013). ^{226}Ra activities were determined using the ^{214}Pb peaks (295 and 352 keV) and ^{214}Bi peak (609 keV) while ^{228}Ra activities were determined using the ^{228}Ac peaks (338, 911 and 969 keV).

3. Results

3.1. Thermal infrared images (TIR)

3.1.1. TIR images in La Palme lagoon

Fig. 2 shows airborne TIR images associated with the karstic groundwater plume that reaches the northern part of La Palme lagoon *via* a small stream. Two TIR images were acquired on 20 September 2012 at different periods of the day, at 9:26 a.m. and 4:55 p.m. The absolute temperatures measured by the TIR camera and in situ temperature sensors do not match precisely (Fig. 2). The TIR camera calculates temperature from Plank's law, taking into account factors including the object distance, relative humidity, atmospheric temperature and emissivity of water in order to correct for atmospheric transmission. Additionally, the temperature sensors (although they were placed in surface waters) record the temperature slightly deeper (top few cm) than the TIR images. However, what is important to study here is the relative temperature difference between pixels. The temperature sensors indicated that the temperature in the mouth of the stream increased from 17.4 °C to 20.1 °C during the day while the interior of the lagoon increased in temperature (15.5 °C to 21.1 °C) with a greater temperature amplitude than that of the stream mouth. The temperature sensors and the TIR images both indicate that the discharging spring water was warmer (17.4 °C) than the lagoon water (15.5 °C) in the morning, whereas the spring water (20.1 °C) was colder than the lagoon water (21.1 °C) in the afternoon. Note that there is a

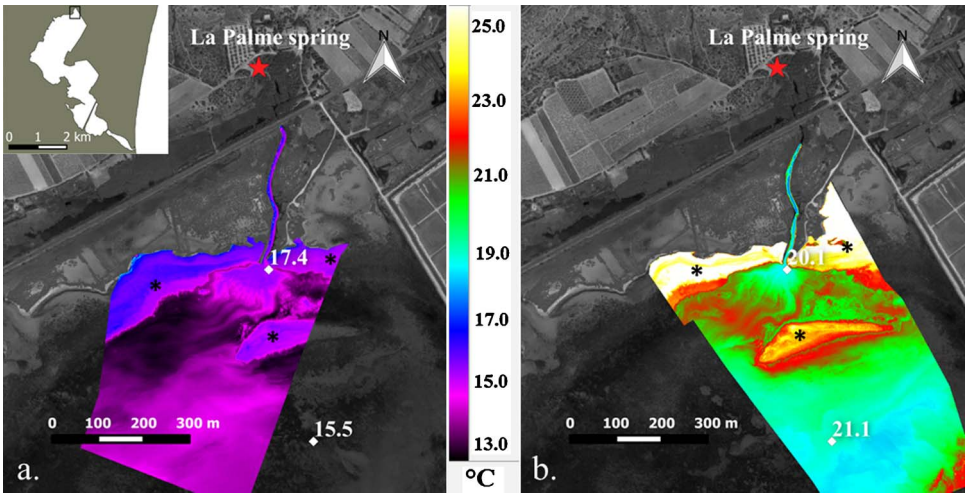

Fig. 2. Airborne thermal infrared images acquired in La Palme lagoon. The two images were obtained at different periods of the day on 20/09/2012, at a) 9:26 a.m. and b) 4:55 p.m. The red star indicates the location of the outlet of the karstic spring (inland) whereas the white diamonds indicate the location of the two temperature sensors placed in the lagoon (at the outlet of the stream and in the middle of the lagoon) to record temperature in parallel to the acquisition of the TIR images. The black stars denote exposed sand areas. The same color scale was applied to the two images to facilitate the comparison. (For interpretation of the references to colour in this figure legend, the reader is referred to the web version of this article.)

sandbar between the two *in situ* sensors and sandy beaches (black stars) on the shore with higher temperature than the water on both images, due to low water level in the lagoon. Depending on the period of the day, the groundwater discharge may therefore be colder or warmer than the surrounding water. This pattern is important to keep in mind when interpreting airborne TIR images.

3.1.2. TIR images in Salses-Leucate lagoon

Fig. 3 shows a TIR image acquired (9:34 a.m.) in the mouth of the stream that connects the Font Estramar spring to the Salses-Leucate lagoon. As was the case in La Palme lagoon, the terrestrial groundwater was warmer than the lagoon water during the morning, as can be seen from the main spring (1.) that discharges into the lagoon. A second plume can also be observed near the mouth of the stream (~100 m southeast, 2.), which was derived from a fish farm that utilizes the karstic spring water before later releasing it into the lagoon. The fish farm does not significantly modify the temperature of the water. As deduced from the TIR image, the surface water temperature of the terrestrial groundwater discharge was 16.5 °C, which is 1 °C warmer than the lagoon water. Another interesting site could be detected during the survey conducted in Salses-Leucate lagoon, where the TIR images clearly show a

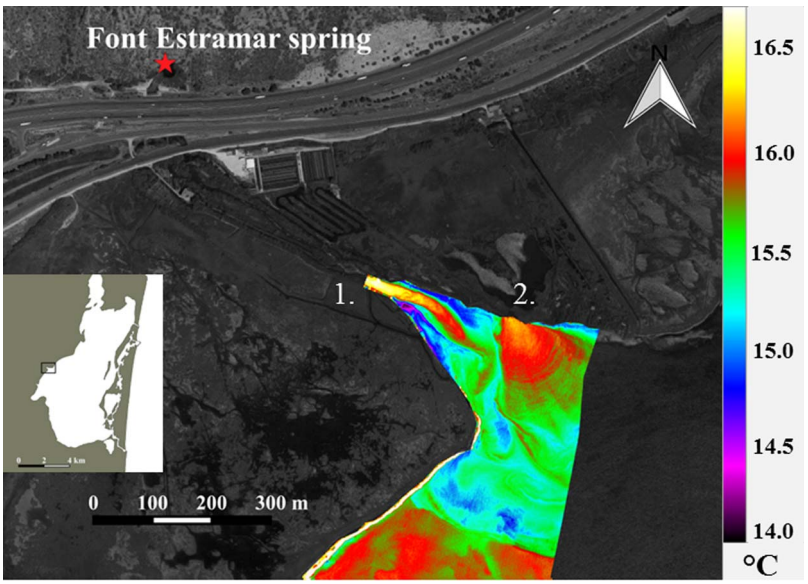

Fig. 3. Airborne thermal infrared image acquired in Salses-Leucate lagoon at 9:34 am on 20/09/2012. The red star indicates the location of the outlet of the Font Estramar spring (inland). The TIR image shows the plume of the stream that connects the spring to the lagoon (1.) and a second plume coming from the fish farm through an artificial channel (2.). (For interpretation of the references to colour in this figure legend, the reader is referred to the web version of this article.)

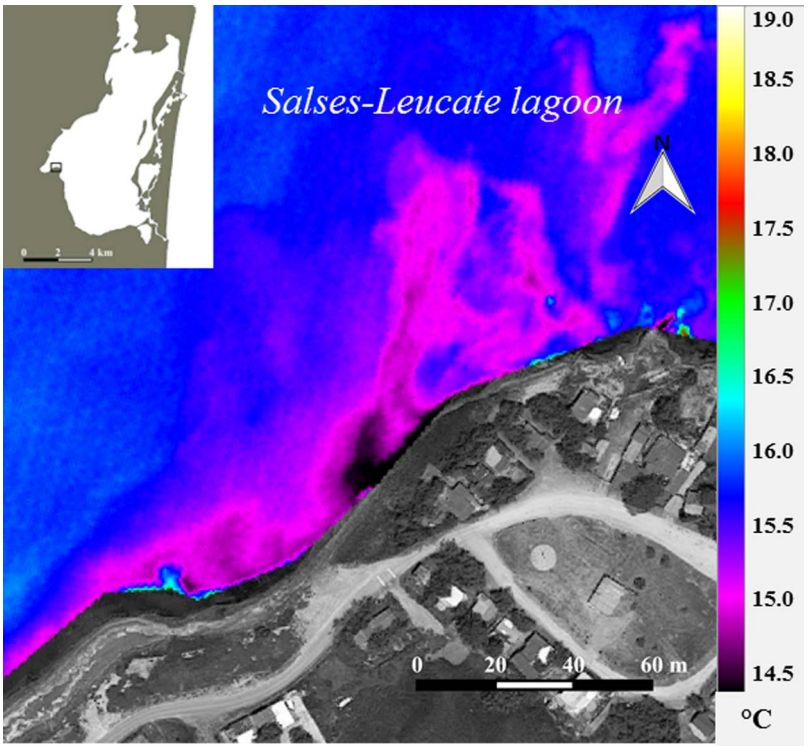

Fig. 4. Airborne thermal infrared image along Salse-Leucate lagoon, acquired at 9:35 am on 20/09/2012.

diffusive flow of terrestrial groundwater that discharged into the southern part of the lagoon (Fig. 4). Salinity and Ra activities were also determined in that location in order to attest that this plume is related to groundwater discharge (Section 3.2.2). Unfortunately, the airborne TIR overflight did not cover the area of the Font Dame spring.

3.1.3. TIR images in Calanques of Marseille-Cassis

Fig. 5 shows TIR images acquired (at ca. 6:00 p.m.) in the Calanques of Marseille-Casssis. Several springs that connect directly to the sea can be identified in this area, where the temperature of the springs that reached the coastal seas appeared colder than the surrounding seawater. The well-known springs located in the Calanque of Port-Miou are readily apparent in the TIR images (Fig. 5d).

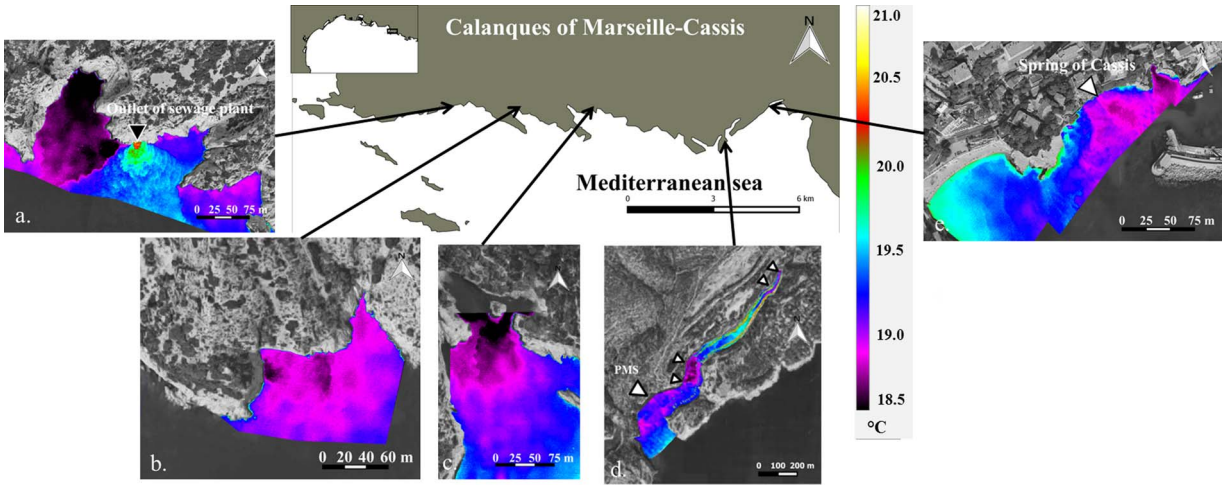

Fig. 5. Airborne thermal infrared images collected at different spots in Calanques de Marseille-Cassis on 20/09/2012 at *circa* 6:00 p.m. TIR images were acquired in a. Calanque of Cortiou, b. Calanque of Sormiou, c. Calanque of Sugiton, d. Calanque of Port Miou and e. Cassis and. The same color scale was used for the different images. The white triangles indicate the location of springs in Calanque of Port Miou according to Gilli (2001), and are scaled to qualitatively reflect the discharge magnitude. PMS indicates the location of Port-Miou spring, the main spring discharging in the Calanque. The black triangle indicates the location of the waste-water effluent (Muricy, 1991).

Table 1
Salinity and radium activities determined in the different springs investigated in this study. The water samples were collected at the outlet of the springs. In some cases, repeated sampling was conducted.

Spring	Latitude (°N)	Longitude (°E)	Sampling Date	Salinity	$^{224}Ra_{ex}$ dpm 100 L^{-1}	$^{223}Ra_{ex}$ dpm 100 L^{-1}	^{226}Ra dpm 100 L^{-1}	^{228}Ra dpm 100 L^{-1}
Spring in La Palme lagoon	42.97870	3.01138	5/13/2009	6.9	458 ± 46	30 ± 3	316 ± 4	188 ± 5
"			6/26/2009	7.4	427 ± 43	18 ± 4	398 ± 4	237 ± 6
"			9/23/2009				263 ± 5	176 ± 7
"			3/1/2016	8.0	587 ± 112	46 ± 11		
"			3/8/2016	8.3	652 ± 78	43 ± 7		
"			4/13/2016	8.8	628 ± 87	16 ± 4	390 ± 6	366 ± 12
Font Estramar spring (Salses-Leucate lagoon)	42.8593	2.95842	3/27/2008	2.6	146 ± 10	4 ± 1	49 ± 1	84 ± 3
"			4/12/2016	3.7	244 ± 30	2 ± 1	68 ± 3	139 ± 8
Font Dame spring (Salses-Leucate lagoon)	42.85050	2.93740	4/12/2016	2.2	140 ± 7	2 ± 1	49 ± 2	74 ± 6
Springs in Calanque of Port-Miou	43.20520	5.51290	7/7/2009	26.9	37 ± 3	7 ± 1	149 ± 2	65 ± 2
"	43.21111	5.52167	7/7/2009	10.1	109 ± 6	17 ± 2	252 ± 2	105 ± 3
"	43.21111	5.52167	7/7/2009	10.0	98 ± 7	12 ± 2	186 ± 2	80 ± 3
Vise spring, 30 m depth	43.45673	3.67945	7/21/2009	2.8	89 ± 6	5 ± 1	81 ± 1	48 ± 2
Vise Spring, surface (Thau lagoon)			7/20/2009	36.3	83 ± 6	9 ± 1	32 ± 1	71 ± 2

Note that there are several small orange lines on Fig. 5d, which represent small boats that line the perimeter of the Calanque. It should be noted that this warm signal can obscure any thermal signature of potential spring inputs in the area. Several other springs could be identified during this survey including Calanque of Sormiou, Calanque of Cortiou, Calanque of Sugiton or the exit of Cassis harbor (Fig. 5). Note that one plume appears warmer than seawater (Fig. 5a), which corresponds to the outlet of the sewage plant of Marseille that is located in Calanque of Cortiou (Muricy, 1991).

3.1.4. TIR data from Thau lagoon

We acquired TIR images in Thau lagoon to attempt to detect the Vise spring located in the northern part of the lagoon off Balaruc-les-Bains. Although the spring is visible at the surface, no temperature signal could be found associated with this spring. Because the outlet of the Vise spring is located at 30 m depth, the waters were likely well-mixed before reaching the surface. In addition, because the Vise spring is a mix of karstic waters, thermal waters and seawater (Aquilina et al., 2002), the waters at the outlet were likely not as cold as the groundwater in the springs discussed above. Therefore, in this specific setting, the application of high-resolution airborne TIR imagery to locate SGD is only suitable to detect terrestrial water fluxes at or near the surface and may not be used to detect deep sources, because deep water mixes rapidly with the surrounding waters, losing its thermal signature.

3.2. Characterization of the different sites: salinity and radium isotopes

To complement the TIR images, we characterized the different sites *in situ* by documenting salinity and Ra isotopes in the springs at their outlets (Table 1). We also investigated the fate of salinity and Ra isotopes during transport between the outlet and lagoon waters or coastal seas (Table 2). In some cases, repeated sampling was conducted as a first attempt to document any temporal variability. We report data for five different springs: the spring in La Palme lagoon, Font Estramar and Font Dame springs (both in Salses-Leucate lagoon), Port-Miou springs (Calanque of Marseille-Cassis) and the Vise spring (Thau Lagoon). The activities reported here range between 2 and 46 dpm 100 L^{-1} for $^{223}Ra_{ex}$; 37–652 dpm 100 L^{-1} for $^{224}Ra_{ex}$; 32–398 dpm 100 L^{-1} for ^{226}Ra and 48–366 dpm 100 L^{-1} for ^{228}Ra. The ^{228}Ra activities reported here compare well with the ^{228}Ra activities reported in different systems along the Mediterranean coastline in Spain, Italy, Greece, France, Tunisia, Egypt and Israel by Rodellas et al. (2015). Our data lie between the first and the third quartile (60–200 dpm 100 L^{-1}) of this ^{228}Ra dataset. $^{223}Ra_{ex}$ and $^{224}Ra_{ex}$ activities are also similar compared with other systems investigated in Castello, Spain (Garcia-Solsona et al., 2010) and Sicily, Italy (Moore, 2006).

3.2.1. La Palme lagoon

In July 2009, we conducted a survey in the entire La Palme lagoon where we measured salinity, $^{223}Ra_{ex}$ and $^{224}Ra_{ex}$ activities (Fig. 6, Table 3). The spatial distribution of salinity, $^{223}Ra_{ex}$ and $^{224}Ra_{ex}$ activities are shown in Fig. 6. Higher Ra activities and lower salinity waters were found in the northern part of the lagoon, as a result of terrestrial groundwater inputs in that area from the spring (LAP 21, Fig. 6a; see also Figs. 2 and 7). In the intermediate basin, activities remained lower (one order of magnitude less than the northern part of the basin and 2–3 times lower than the southern basin). The Ra activities increased again in the southern part of the lagoon, suggesting that significant seawater recirculation occurred near the sandy, permeable area where the lagoon connects to the sea, as (i) there are no known groundwater inputs in this region and (ii) surface water salinities reflected those of the open Mediterranean Sea. This latter pattern was also observed with ^{222}Rn (Stieglitz et al., 2013).

The salinity of La Palme spring varied between 6.9 and 8.8 at its outlet (Table 1), and suggests significant mixing of groundwater with seawater in the aquifer. This spring displays the highest Ra activities for all four Ra isotopes among the different systems investigated here, with activities reaching 46, 652, 398 and 366 dpm 100 L^{-1} for $^{223}Ra_{ex}$, $^{224}Ra_{ex}$, ^{226}Ra and ^{228}Ra, respectively. The

Table 2
Salinity, Ra activities and Ra activity ratios determined in Calanque of Port-Miou in July 2009 and in the different streams that connect the springs to the lagoons in April 2016.

Location	Samples ID	Latitude (°N)	Longitude (°E)	Salinity	$^{224}Ra_{ex}$ dpm 100 L^{-1}	^{228}Ra dpm 100 L^{-1}	$^{224}Ra_{ex}/^{228}Ra$
Calanque of Port-Miou	CAL1	43.20250	5.51361	32.1	20 ± 2	24 ± 1	0.83 ± 0.09
"	CAL2	43.20483	5.51257	30.8	28 ± 3	37 ± 2	0.75 ± 0.08
"	CAL3	43.20528	5.51333	27.8	35 ± 3	45 ± 2	0.76 ± 0.07
"	CAL4	43.20543	5.51385	29.1	27 ± 3	49 ± 2	0.56 ± 0.06
"	CAL5	43.20556	5.51444	28.8	34 ± 3	45 ± 2	0.76 ± 0.08
"	CAL6	43.20588	5.51564	n.d	52 ± 4	76 ± 2	0.68 ± 0.05
"	CAL7[a]	43.21132	5.52106	10.1	109 ± 6	105 ± 3	1.04 ± 0.07
"	CAL8	43.21121	5.52098	10.0	98 ± 7	80 ± 3	1.22 ± 0.09
"	CAL9	43.21125	5.52128	14.3	100 ± 5	104 ± 3	0.96 ± 0.06
"	CAL10	43.20524	5.51295	26.9	37 ± 3	65 ± 2	0.56 ± 0.05
"	CAL11[b]	43.20167	5.51472	34.2	12 ± 1	13 ± 1	0.89 ± 0.11
"	CAL12	43.20789	5.51788	26.3	44 ± 3	57 ± 2	0.76 ± 0.06
"	CAL13	43.20925	5.51949	28.0	38 ± 3	40 ± 2	0.95 ± 0.08
"	CAL14	43.21033	5.52074	25.6	65 ± 4	72 ± 2	0.91 ± 0.07
Stream in La Palme lagoon	LAP1[c]	42.97878	3.01138	8.8	628 ± 87	366 ± 12	1.71 ± 0.24
"	LAP3	42.97840	3.01183	8.8	709 ± 107	387 ± 12	1.83 ± 0.28
"	LAP4	42.97802	3.01186	8.8	815 ± 149	420 ± 13	1.94 ± 0.36
"	LAP5	42.97560	3.01188	9.7	733 ± 99	419 ± 13	1.75 ± 0.24
"	LAP6	42.97494	3.01164	12.6	561 ± 74	392 ± 12	1.43 ± 0.19
"	LAP7	42.97461	3.01150		91 ± 6	154 ± 8	0.59 ± 0.05
"	LAP8[d]	42.97183	3.01077	28.5	68 ± 4	124 ± 7	0.55 ± 0.04
Font Estramar stream	LEUC1	42.85735	2.95969	3.8	249 ± 16	167 ± 9	1.49 ± 0.12
(Salses-Leucate lagoon)	LEUC2	42.85720	2.96015	3.7	220 ± 16	144 ± 8	1.53 ± 0.14
"	LEUC3	42.85651	2.96167	4.8	178 ± 32	170 ± 8	1.05 ± 0.20
"	LEUC4	42.85614	2.96219	5.5	209 ± 13	157 ± 8	1.33 ± 0.11
"	LEUC5	42.85595	2.96275	7.3	216 ± 12	150 ± 8	1.44 ± 0.11
"	LEUC6	42.85605	2.96301	10.7	238 ± 31	153 ± 8	1.55 ± 0.22
"	LEUC7	42.85466	2.96577	24.3	204 ± 12	123 ± 7	1.65 ± 0.14
"	LEUC8[e]	42.85327	2.96891	33	83 ± 7	83 ± 6	1.00 ± 0.11
"	LEUC12[f]	42.85930	2.95843	3.7	244 ± 30	139 ± 8	1.75 ± 0.24
"	LEUC13	42.85920	2.95851	3.7	245 ± 30	172 ± 9	1.42 ± 0.19
"	LEUC14	42.85815	2.95826	3.7	229 ± 18	171 ± 9	1.34 ± 0.12
Font Dame stream	LEUC9	42.84410	2.95375	9.4	114 ± 20	90 ± 7	1.27 ± 0.24
(Salses-Leucate lagoon)	LEUC10	42.84728	2.94054	2.3	114 ± 7	82 ± 6	1.39 ± 0.13
"	LEUC11[g]	42.85052	2.93745	2.2	140 ± 7	74 ± 6	1.89 ± 0.17
"	LEUC16	42.84663	2.94324	7.3	136 ± 24	64 ± 5	2.14 ± 0.43
"	LEUC17	42.84638	2.94474	7.4	117 ± 8	77 ± 6	1.52 ± 0.16
"	LEUC18	42.84649	2.94633	7.8	132 ± 8	64 ± 5	2.06 ± 0.21
"	LEUC19	42.84612	2.94817	8.2	138 ± 18	76 ± 6	1.82 ± 0.28
"	LEUC20	42.84524	2.95105	9.1	118 ± 8	76 ± 6	1.55 ± 0.16
"	LEUC21	42.84387	2.95428	17.9	110 ± 9	91 ± 6	1.20 ± 0.12
"	LEUC22	42.84306	2.95549	28.7	101 ± 19	115 ± 7	0.87 ± 0.17

n.d.: not determinded.
[a] is the groundwater endmember of the calanque of Port-Miou.
[c] is the endmember of the stream in La Palme lagoon.
[f] is the endmember of the Font Estramar stream.
[g] is the endmember of the Font Dame stream. These endmembers are used to determine the apparent water ages.
[b] is the seawater endmember for the Calanque of Port-Miou.
[d] is the lagoon water endmember for La Palme lagoon.
[e] is the lagoon water endmember for Salses-Leucate lagoon.

spring water was collected at different periods of the year in 2009 and 2016. Although activities of the four Ra isotopes remain high, significant temporal variability was observed.

Fig. 7 shows the spatial distribution of salinity and $^{224}Ra_{ex}$ activities along the stream that connects the spring to La Palme lagoon in April 2016. The salinity along the stream slightly increased from 8.8 to 12.6 in the stream mouth and was 28.5 in the lagoon (Fig. 7a). Here we report only the $^{224}Ra_{ex}$ activities, because ^{224}Ra, with its short half-life, is best adapted to study the timescale of groundwater discharge into the lagoon waters. The $^{224}Ra_{ex}$ activities decreased from 628 dpm 100 L^{-1} at the outlet of the spring to 561 dpm 100 L^{-1} in the stream mouth, whereas $^{224}Ra_{ex}$ activities were 68 dpm 100 L^{-1} in the lagoon. Note that the $^{224}Ra_{ex}$ activities were not highest at the outlet of the spring. Additional inputs of ^{224}Ra along the stream may not be completely excluded (e.g., additional groundwater input; desorption of Ra from suspended particles; sediment inputs). Fig. 7c shows the $^{224}Ra_{ex}$ activities as a function of the salinity along the stream.

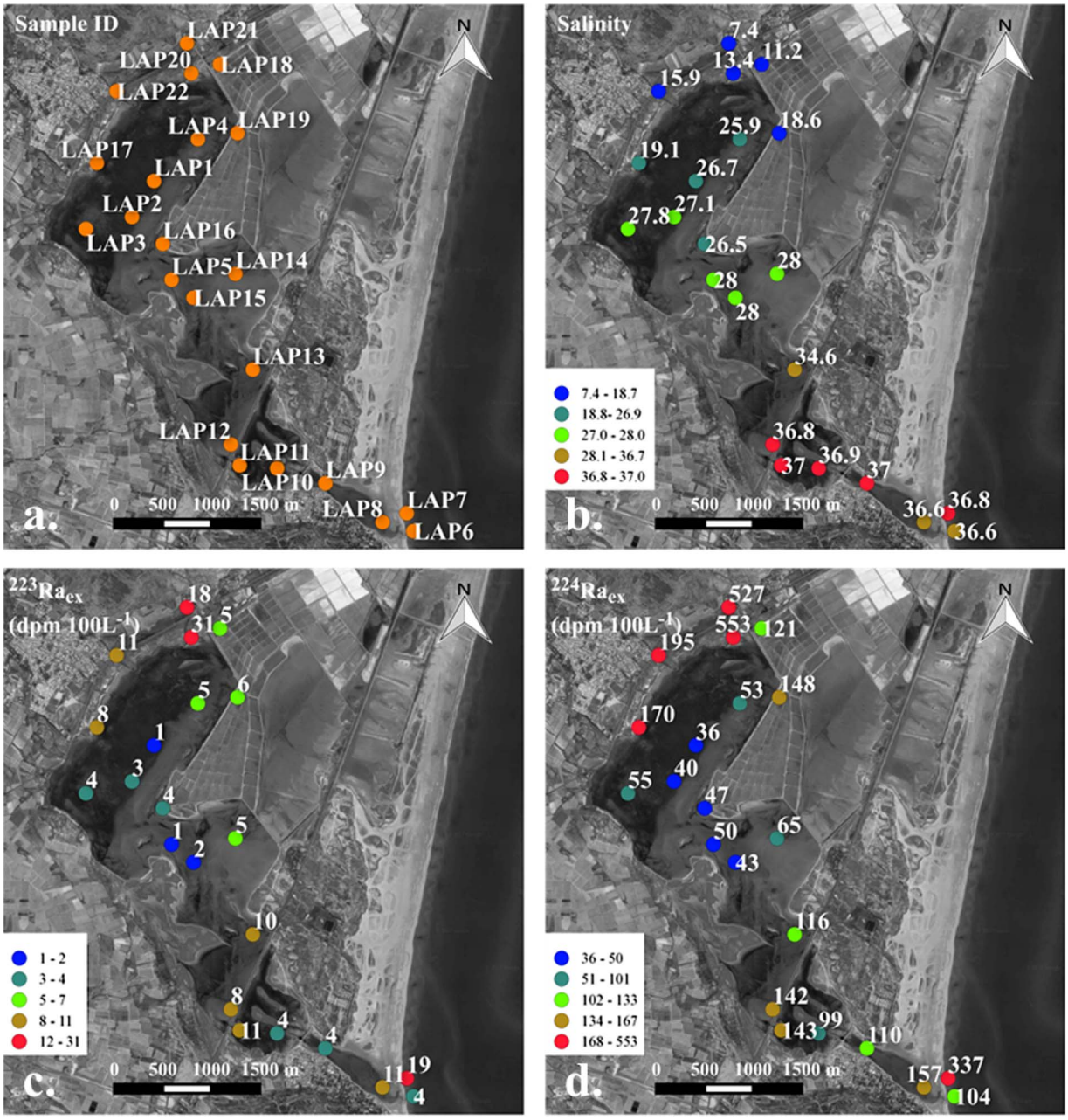

Fig. 6. a. Stations investigated in the La Palme lagoon and b. the salinity, c. $^{223}Ra_{ex}$ activity and d. $^{224}Ra_{ex}$ activity determined in these samples collected in June 2009. Note that the color scale is non-linear.

3.2.2. Salses-Leucate lagoon

Fig. 8 shows the spatial distribution of salinity and $^{224}Ra_{ex}$ activities along the streams that connect the springs to Salses-Leucate lagoon in April 2016. The Font Estramar and Font Dame springs salinities in April 2016 were 3.7 and 2.2 respectively. The salinity ranged from 3.7–24.3 in the stream that connects Font Estramar to the lagoon, whereas the salinity in the lagoon slightly offshore was 33 (Fig. 8a). The salinity in the stream that connects Font Dame to the lagoon ranged from 2.2–28.7 (Fig. 8d). The $^{224}Ra_{ex}$ activities varied between 244 dpm 100 L^{-1} at the outlet of the Font Estramar spring to 204 dpm 100 L^{-1} in the mouth of stream. The $^{224}Ra_{ex}$ activities ranged between 140 dpm 100 L^{-1} at the outlet of the Font Dame spring to 101 dpm 100 L^{-1} in the mouth of stream. The Ra activities at the outlet of these two springs were lower than the activities reported for the karstic spring in La Palme lagoon (Table 1). The highest $^{224}Ra_{ex}$ activity in the Font Estramar system was not found at the outlet of the spring. Similar to La Palme lagoon, additional inputs of ^{224}Ra along the stream may not be completely excluded. The $^{224}Ra_{ex}$ activities in the Font Estramar and Font Dame systems, between the outlet of the springs and the lagoon, are shown as a function of salinity (Fig. 8c and f). The decreasing

Table 3
Surface water radium activities determined in La Palme lagoon in June 2009.

Samples ID	Latitude (°N)	Longitude (°E)	Salinity	$^{224}Ra_{ex}$ dpm 100 L^{-1}	$^{223}Ra_{ex}$ dpm 100 L^{-1}
LAP1	42.96583	3.00778	26.7	36 ± 3	1 ± 1
LAP2	42.96250	3.00500	27.1	40 ± 4	3 ± 1
LAP3	42.96139	2.99917	27.8	55 ± 5	4 ± 1
LAP4	42.96972	3.01333	25.9	53 ± 4	5 ± 1
LAP5	42.95667	3.01000	28.0	50 ± 4	1 ± 1
LAP6[a]	42.93333	3.04056	36.6	104 ± 7	4 ± 1
LAP7	42.93500	3.03972	36.8	337 ± 23	19 ± 4
LAP8	42.93417	3.03667	36.6	157 ± 11	11 ± 2
LAP9	42.93778	3.02944	37.0	110 ± 7	4 ± 1
LAP10	42.93917	3.02333	36.9	99 ± 5	4 ± 1
LAP11	42.93944	3.01861	37.0	143 ± 8	11 ± 2
LAP12	42.94139	3.01750	36.8	142 ± 9	8 ± 1
LAP13	42.94833	3.02028	34.6	116 ± 5	10 ± 1
LAP14	42.95722	3.01806	28.0	65 ± 5	5 ± 1
LAP15	42.95500	3.01278	28.0	43 ± 4	2 ± 1
LAP16	42.96000	3.00889	26.5	47 ± 3	4 ± 1
LAP17	42.96750	3.00056	19.1	170 ± 13	8 ± 2
LAP18	42.97667	3.01611	11.2	121 ± 6	5 ± 1
LAP19	42.97028	3.01833	18.6	148 ± 9	6 ± 1
LAP20	42.97583	3.01250	13.4	553 ± 39	31 ± 4
LAP21[b]	42.97861	3.01194	7.4	527 ± 43	18 ± 4
LAP22	42.97417	3.00306	15.9	195 ± 16	11 ± 3

[a] is the seawater endmember.
[b] is the groundwater endmember.

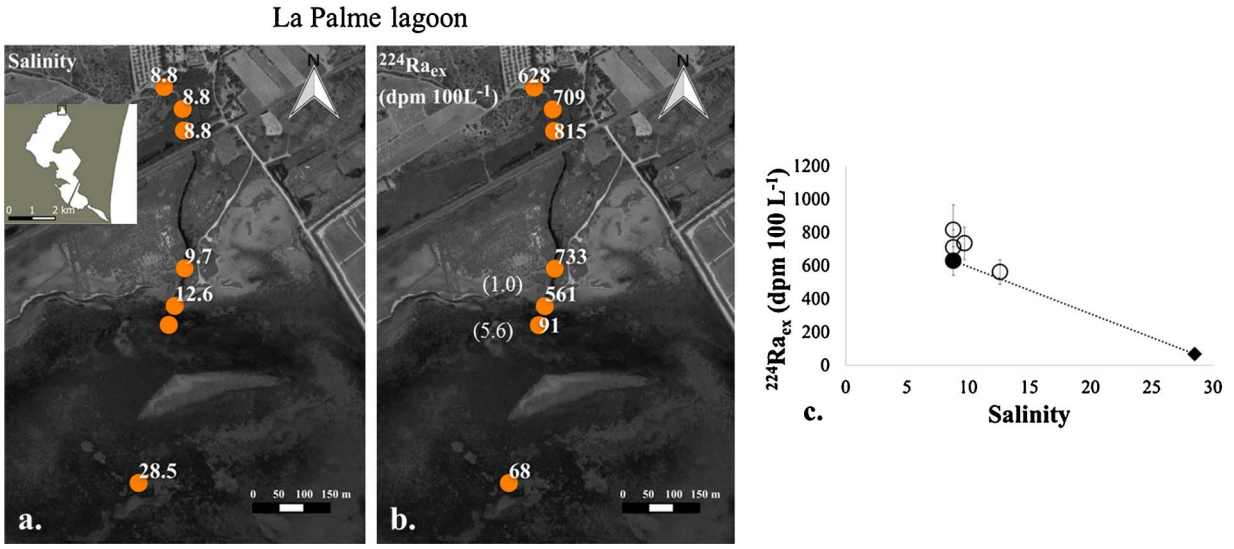

Fig. 7. Distribution of a. salinity and b. $^{224}Ra_{ex}$ activities determined along the stream that connects the karstic spring (inland) to La Palme lagoon. Samples were collected in April 2016. The Ra apparent water ages (days) derived from the $^{224}Ra_{ex}/^{228}Ra$ ratios (Table 2), which are used in the water flux calculations, are displayed in parentheses. Along the stream, we only report ages that are significantly different from zero (i.e., samples displaying $^{224}Ra_{ex}/^{228}Ra$ ratios significantly lower than the endmember ratio due to radioactive decay). c. Relationship between $^{224}Ra_{ex}$ and salinity for the same samples. The filled circle represents the groundwater spring endmember (Table 2); the filled diamond represents the lagoon water endmember; the dotted line represents the mixing line between the spring and lagoon water.

trend is similar to that in La Palme (Fig. 7c). The general decreasing trend in the $^{224}Ra_{ex}$ activities along the streams may be related to radioactive decay and mixing with lagoon waters.

Finally, we determined the Ra activities and salinity in samples collected in the southern part of the Salses-Leucate lagoon where a TIR signal was detected (Fig. 4). Surface water samples taken along the shoreline within the TIR anomaly had slightly lower salinities (from 28.8 to 29.6; n = 5) than that of waters in the center of the lagoon (ca. 33). The $^{224}Ra_{ex}$ activities were within 110–499 dpm 100 L^{-1} (n = 5), while the $^{223}Ra_{ex}$ activities were within 7–11 dpm 100 L^{-1} (n = 5). These activities were well above the activities determined in the open lagoon and therefore suggest that this area was a site of significant groundwater discharge. There are some ponds inland near this area; we sampled the closest pond and found that the salinity was higher (30.9) than the main body of the lagoon. This information, coupled with the radionuclide data, suggest that the observed TIR anomalies are not sourced from this pond

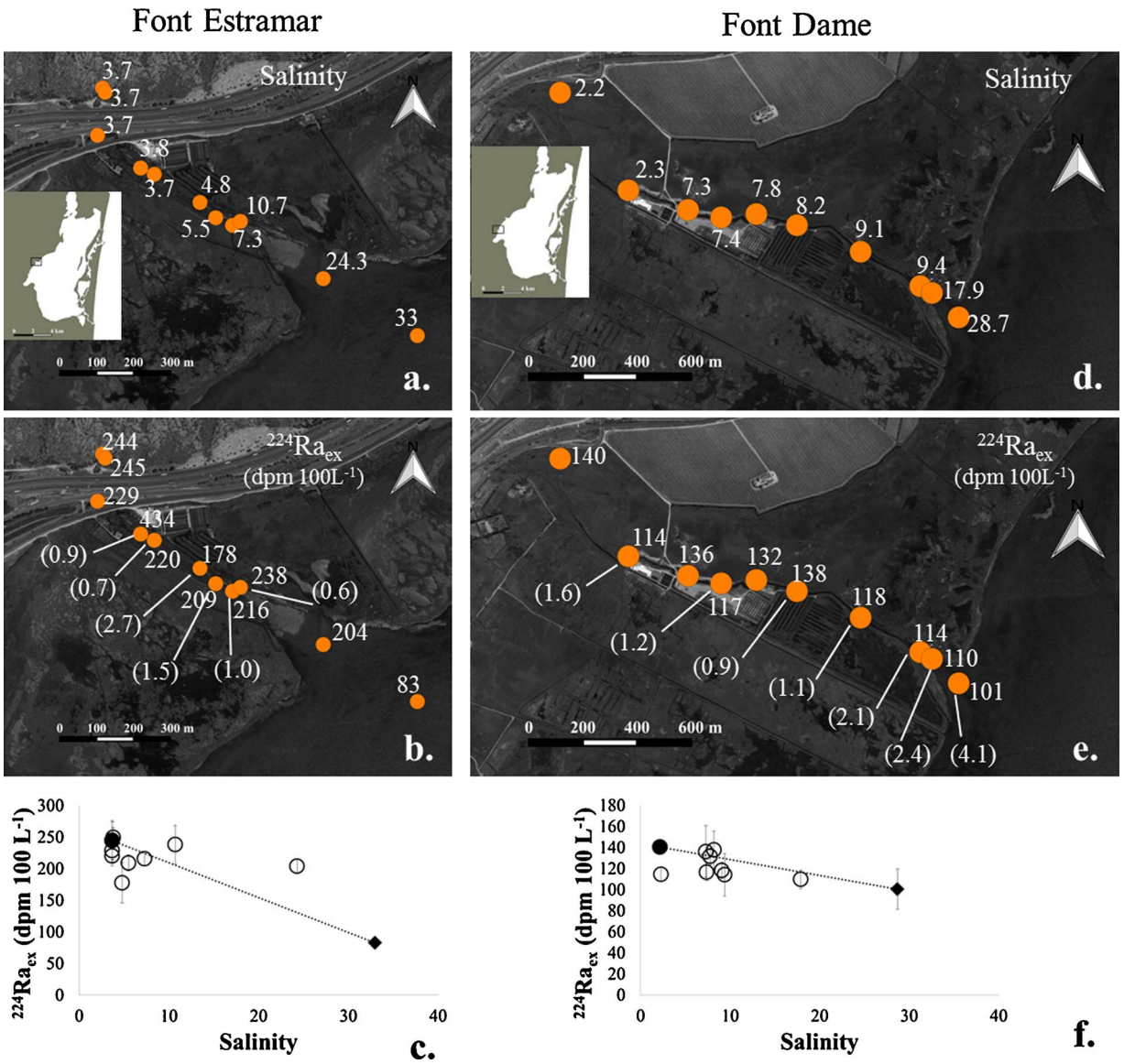

Fig. 8. Distribution of a. salinity and b. $^{224}Ra_{ex}$ activities determined along the stream that connects the Font Estramar spring to the Salses-Leucate lagoon and d. salinity and e. $^{224}Ra_{ex}$ activities determined along the stream that connects the Font Dame spring (inland) to the Salses-Leucate lagoon. Samples were collected in April 2016. The Ra apparent water ages (days) derived from the $^{224}Ra_{ex}/^{228}Ra$ ratios (Table 2), which are used in the water flux calculations, are displayed in parentheses. Along the stream, we only report ages that are significantly different from zero (i.e., samples displaying $^{224}Ra_{ex}/^{228}Ra$ ratios significantly lower than the endmember ratio due to radioactive decay). c. and f. Relationship between $^{224}Ra_{ex}$ and salinity for the same samples, respectively. The filled circle represents the groundwater spring endmember (Table 2); the filled diamond represents the lagoon water endmember; the dotted line represents the mixing line between the spring and lagoon water.

and that there is likely negligible exchange between the adjacent ponds and Salses-Leucate lagoon at this site.

3.2.3. *Calanque of Port-Miou*

Fig. 9 displays the distribution of salinity and radium isotopes along the Calanque of Port-Miou (Fig. 5d). The Ra activities are highest for all four isotopes in the northern part of the Calanque, where activities reach 18, 109, 252 and 105 dpm 100 L^{-1} for $^{223}Ra_{ex}$, $^{224}Ra_{ex}$, ^{226}Ra and ^{228}Ra, respectively. These activities are relatively high as a result of groundwater inputs in the northern most part of the Calanque of Port-Miou (Fig. 5d; Arfib et al., 2006). The general trend is that salinity increases while Ra activities decrease when moving from the northern part of the Calanque towards its mouth. This is despite the fact that groundwater also discharges at the entrance of the Calanque (e.g., CAL10 was collected in front of the main outlet) where activities reached 7, 37, 149 and 65 dpm 100 L^{-1} for $^{223}Ra_{ex}$, $^{224}Ra_{ex}$, ^{226}Ra and ^{228}Ra, respectively (Table 1). In contrast, Ra activities outside of the bay were 2, 12, 35 and 13 dpm 100 L^{-1} for $^{223}Ra_{ex}$, $^{224}Ra_{ex}$, ^{226}Ra and ^{228}Ra, respectively. The activities at the spring outlets therefore denote a clear Ra enrichment in comparison to the seawater activities. However, the narrow section in the northern part of the Calanque likely

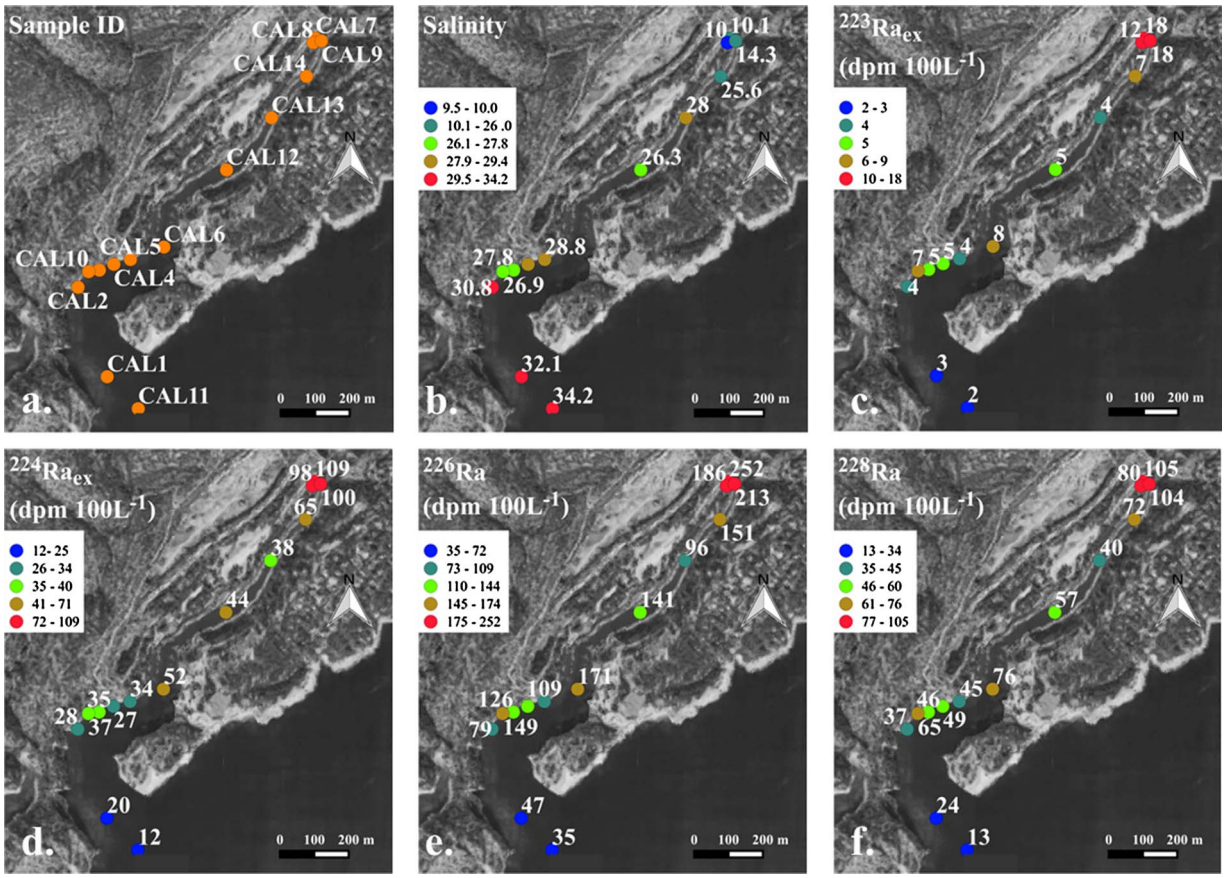

Fig. 9. a. Stations investigated in Calanque of Port-Miou and b. salinity, c. $^{223}Ra_{ex}$, d. $^{224}Ra_{ex}$, e. ^{226}Ra and f. ^{228}Ra activities (dpm 100 L^{-1}) determined in the Calanque of Port-Miou. Samples were collected in July 2009. Note that the color scale is non-linear.

limits mixing between seawater and terrestrial groundwater, whereas mixing with seawater was likely more efficient in the southern part due to the wider opening of the Calanque, thus diluting the signal associated with groundwater (Ra activity, salinity). Ra activities generally lie on a mixing line between spring and seawater endmembers (Fig. 10). Activities observed above the mixing line (e.g. ^{226}Ra and ^{228}Ra towards the mouth of Calanque) may indicate an additional input of Ra associated with the springs that discharge towards the mouth of the Calanque, for example, from a temporally-variable spring which discharged at some time before sampling and then ceased or reduced in flow. Under this scenario, the short-lived Ra isotopes would have decayed on the time-scale of several days to weeks, and therefore lie on the mixing line, while the long lived isotopes would be enriched relative to the mixing line if mixing processes were relatively slow.

3.2.4. Thau lagoon

In Thau lagoon, water from the Vise spring was collected both at its outlet at 30 m depth by two divers (Thierry Laugier, IFREMER and Pascal Brunet, HSM) and in surface waters just above the outlet. The salinity at the outlet was 2.8, whereas 30 m above at the surface, the salinity was already 36.3, thus highlighting the fast mixing of the groundwater during transport to the surface. As discussed above, the temperature signal was lost during upward transport, which prevented us from detecting the plume at the surface using TIR remote sensing. The Ra activities associated with the Vise spring at its outlet in the lagoon were among the lowest of the different systems described here, with activities of 5, 89, 81 and 48 dpm 100 L^{-1} for $^{223}Ra_{ex,}$ $^{224}Ra_{ex}$, ^{226}Ra and ^{228}Ra, respectively (Table 1). These activities were an order of magnitude lower than the activities determined in several thermal springs studied in the area of Balaruc-Les-Bains near the Vise spring (Condomines et al., 2012). Activity Ratios (AR) in these thermal springs were in some cases close to those determined in the Vise spring at its outlet (i.e.$^{228}Ra/^{226}Ra$ AR of 0.59 ± 0.02 for the Vise spring and 0.58 ± 0.02 in the thermal springs; $^{223}Ra/^{224}Ra$ AR of 0.05 ± 0.01 in the Vise spring while it varies from 0.02 to 0.24 in the thermal springs). In contrast, the $^{224}Ra/^{228}Ra$ AR was higher within the Vise spring (1.88 ± 0.14), whereas Condomines et al. (2012) reported AR ranging from 0.62 to 1.34 in the thermal springs. This pattern agrees with the view that the Vise spring is composed of waters of different origins, including karstic water and thermal water (Aquilina et al., 2002; Condomines et al., 2012).

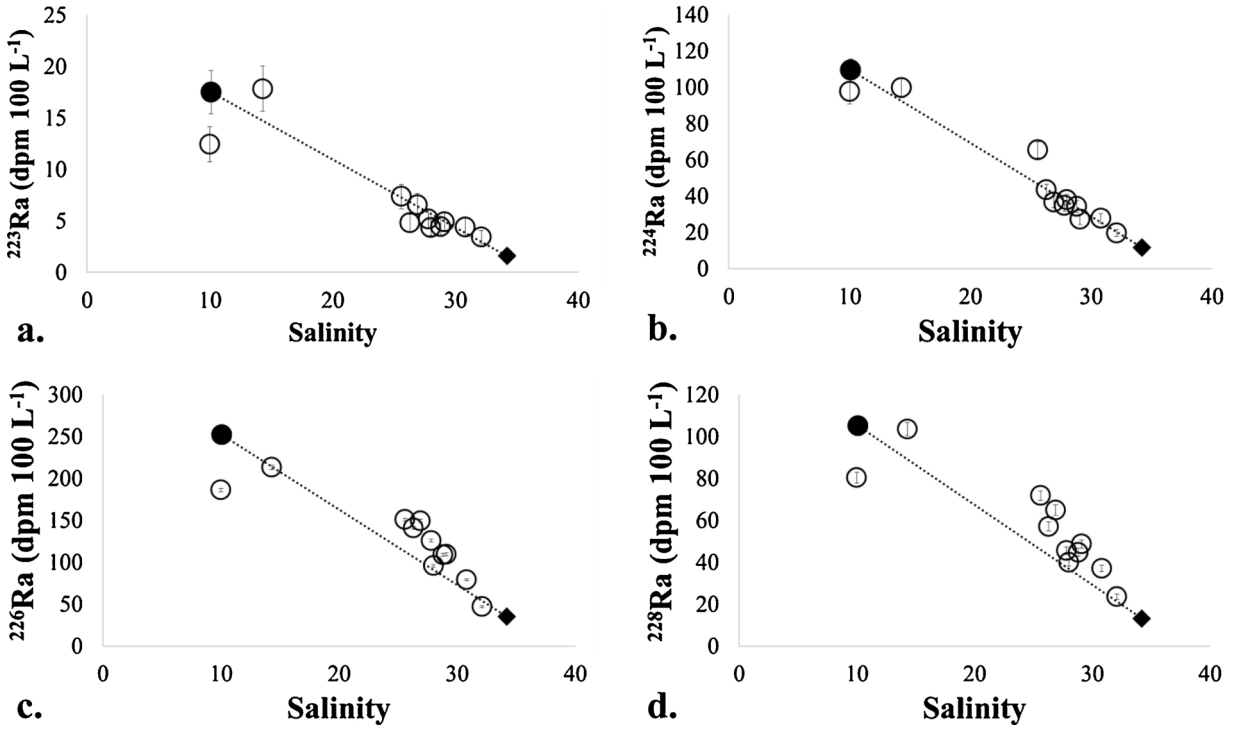

Fig. 10. a. $^{223}Ra_{ex}$, b. $^{224}Ra_{ex}$, c. ^{226}Ra and d. ^{228}Ra activities as a function of salinity in surface water samples collected in the Calanque of Port-Miou. Samples were collected in July 2009. The filled circle represents the groundwater spring endmember; the filled diamond represents the seawater endmember; the dotted line represents the mixing line between the spring and seawater. Note that symbols are often larger than error bars.

4. Discussion

After having characterized the different sites along the French Mediterranean coastline (TIR images, Ra isotopes, salinity), we now use the Ra activities to provide quantitative information in the various systems investigated here.

4.1. Estimate of apparent water ages and water fluxes

Radium isotopes can be used as chronometers to derive apparent water ages that provide estimates of water residence time. In the different investigated systems, we determined the apparent water ages derived from the $^{224}Ra_{ex}/^{228}Ra$ activity ratios (AR) following Moore (2000):

$$t = \frac{[\frac{^{224}Ra}{^{228}Ra}]_i}{[\frac{^{224}Ra}{^{228}Ra}]_{obs}} \times \frac{1}{\lambda_{224} - \lambda_{228}} \quad (1)$$

Where $(^{224}Ra/^{228}Ra)_i$ is the initial ratio in the spring at its outlet, $(^{224}Ra/^{228}Ra)_{obs}$ is the ratio for a given water sample, λ_{224} and λ_{228} are the decay constants of ^{224}Ra and ^{228}Ra, respectively.

Here we assumed that mixing processes (i.e. mixing between groundwater and lagoon water along the streams) do not impact the $^{224}Ra/^{228}Ra$ ratio along the stream. Note that we evaluated the impact of mixing of terrestrial groundwater with lagoon water on the ^{224}Ra and ^{228}Ra activities using a simple two end-member mixing model. We found that the correction for the Ra activities associated with the lagoon water has only a minor impact on the Ra ratios determined along the streams and therefore a minor impact on the derived apparent water ages. The ages reported here along the streams are thus derived from the $^{224}Ra_{ex}/^{228}Ra$ ratio without any correction for mixing processes. For the three systems investigated here, we choose the springs sampled in April 2016 as endmembers as they were sampled at the same time as the surface water samples used to calculate the apparent water ages. Using Eq. (1), the apparent water ages determined in the stream mouth in La Palme lagoon were in the range 1.0–5.6 days (Fig. 7b). Terrestrial groundwater thus reaches La Palme lagoon on a timescale of less than 6 days. Considering the distance between the outlet and the stream mouth, the stream velocity is therefore 132–740 m d^{-1} for these two apparent water ages. Stream velocity should be relatively constant over this small time-scale; therefore, the range of velocities reported here reflects the uncertainties (choice of the endmember and mixing assumption) associated with the assumptions used in the apparent water age calculations. We can then calculate the terrestrial groundwater flux considering the terrestrial groundwater impacted area of the stream. The width of the stream was measured in the field while the thickness of the groundwater layer was estimated to be approximately 20 cm, lying on top

of brackish water. This thickness was measured in the field with a salinity probe. This yields a groundwater flow of $\leq 0.012\ m^3\ s^{-1}$ ($\leq 1036\ m^3\ d^{-1}$) for the spring that connects to La Palme lagoon (April 2016). Measurements conducted with a flow-meter in La Palme spring in September 2016 yielded a flow in the range 0.01–0.02 $m^3\ s^{-1}$. These values are in fair agreement with our upper-bound estimate derived from radium isotopes.

Apparent water ages were also determined using the $^{224}Ra_{ex}/^{228}Ra$ ratios along the streams that connect the Font Estramar and Font Dame springs to the Salses-Leucate lagoon. Apparent water ages determined along the streams were 0.6–2.7 days for Font Estramar (Fig. 8b) and 0.9–4.1 days for Font Dame (Fig. 8e), suggesting that the terrestrial groundwater reaches the lagoon on a timescale of less than 3 days for the Font Estramar stream and less than 4.5 days for the Font Dame stream. The stream velocity is thus $\leq$ 1383 m d^{-1} for the Font Estramar stream and $\leq$2644 m d^{-1} for the Font Dame stream. Considering a terrestrial groundwater layer of approximately 20 cm flowing on top of the brackish water, this results in water fluxes of $\leq 0.029\ m^3\ s^{-1}$ ($\leq 2490\ m^3\ d^{-1}$) for the Font Estramar spring and of $\leq 0.055\ m^3\ s^{-1}$ ($\leq 4760\ m^3\ d^{-1}$) for the Font Dame spring, both estimates being determined in April 2016. The water flow along the western shoreline of Salses-Leucate lagoon (Fig. 4) can be quantified using a simple Ra mass balance (Peterson et al., 2008). Assuming an average water depth of 1.0 m (entire lagoon average ~1.7 m), and a calculated mean $^{224}Ra/^{223}Ra$ apparent water age of 2.1 d, the specific discharge rate is approximately 0.069 m d^{-1}. Distributed over the TIR plume area, this would correspond to a groundwater input of 0.015 $m^3\ s^{-1}$, similar to the Font Dame spring. The sum of these flows represents 0.6–1.7% of the average flow of the Agly River (Serrat, 1999) flowing near this area and only 0.08–0.25% of the Aude River (Ludwig et al., 2009), which is the most important river of the area.

Finally, apparent water ages were determined in the northern part of the Calanque of Port-Miou, which receives known groundwater inputs (Fig. 5d). Therefore, the endmember AR can be easily determined for that part of the Calanque. When moving towards the mouth of the Calanque, the mixed-waters have multiple sources, therefore, it is difficult to determine water ages using a single AR. Considering CAL7 as the groundwater endmember (Fig. 9a), we estimated apparent ages of 0.7 days for sample CAL14 and 1.6 days for sample CAL12.

The results from this study demonstrate that terrestrial SGD along the French Mediterranean coastline is volumetrically small compared to the regional river discharge. These terrestrial SGD estimates are in relative agreement with other coastal settings (Burnett et al., 2006), including continental-scale terrestrial SGD estimates which suggest that terrestrial SGD is between 1 and 2% of continental-scale riverine inputs (Sawyer et al., 2016). Similarly, terrestrial SGD into the entire Mediterranean Sea is on the order of 1–25% of the regional river discharge (Rodellas et al., 2015). Future work is needed to determine the relative importance of groundwater solute fluxes on coastal biogeochemical processes.

4.2. Estimate of the SGD flux in La Palme lagoon using a Ra mass balance

We estimate the SGD flux into La Palme lagoon using a Ra mass balance (using $^{223}Ra_{ex}$ and $^{224}Ra_{ex}$ as tracers of SGD inputs). This approach does not discriminate between the terrestrial groundwater inputs and seawater recirculation through permeable sediments (marine groundwater). We can use the Ra activities determined in the lagoon to estimate a Ra flux that can, in turn, be converted into a SGD flux. Assuming steady state, the inputs of Ra are equal to Ra losses, and the Ra mass balance is:

$$J_{SGD} + J_{river} + J_{diff} = J_{decay} + J_{out} \quad (2)$$

Where J_{river} is the Ra flux from the rivers; J_{diff} is the diffusive flux of radium out of the sediment. Diffusion is defined as the transfer of molecules or atoms from a region of high concentration (the sediments) to a region of low concentration (the overlying water). J_{decay} is the Ra loss *via* radioactive decay; J_{out} is the Ra flux from the lagoon to the sea and J_{SGD} is the Ra flux associated with SGD. In July 2009, the connection with the sea was closed and there was no water input associated with rivers (dry season), aside from the stream that connects the spring to the lagoon (i.e. Fig. 7). Therefore, Eq. (2) simplifies to:

$$J_{SGD} + J_{diff} = J_{decay} \quad (3)$$

We estimate the volume of the lagoon (V_{lagoon}) by multiplying the area of the lagoon (4.98 $*10^6\ m^2$) to the average water level in the lagoon during this period (ca. 0.8 m). The Ra loss *via* radioactive decay in the lagoon can be calculated following:

$$J_{decay} = V_{lagoon} \times C_{lagoon} \times \lambda_{Ra} \quad (4)$$

Where C_{lagoon} is the average radium activity in the lagoon and λ_{Ra} is the decay constant of each nuclide. The Ra loss associated with radioactive decay is thus 1.7 $*10^7$ dpm d^{-1} for ^{223}Ra and 9.2 $*10^8$ dpm d^{-1} for ^{224}Ra (Table 4). As we did not determine the Ra diffusive flux in La Palme lagoon, we use Ra diffusive fluxes from the literature. We use values of 1.1–1.7 dpm $m^2\ d^{-1}$ for ^{223}Ra and 32–53 dpm $m^2\ d^{-1}$ for ^{224}Ra from coastal lagoons with similar bottom-sediments (Beck et al., 2008; Garcia-Solsona et al., 2008b). The diffusive flux in La Palme lagoon is thus calculated by multiplying these flux estimates by the area of bottom-sediments that make up La Palme lagoon.Accordingly, diffusive fluxes varied between (5.5–8.4) $*10^6$ dpm d^{-1} for ^{223}Ra and (1.6–2.6) $*10^8$ dpm d^{-1} for ^{224}Ra (Table 4).

From Eq. (4), the SGD flux was (0.9–1.1) $*10^7$ dpm d^{-1} for ^{223}Ra and (6.5–7.6) $*10^8$ dpm d^{-1} for ^{224}Ra. Using the Ra flux and the Ra activity in the SGD endmember (i.e., spring located inland, north of the lagoon; Table 1), we estimate a SGD flux of 0.6–0.8 $m^3\ s^{-1}$ derived from ^{223}Ra and of 1.4–1.7 $m^3\ s^{-1}$ derived from ^{224}Ra (Table 4). This flux is a total SGD flux which is composed of terrestrial groundwater inputs and marine groundwater, which can be driven by different physical processes including wave-set up and wind-driven advection. This mass balance may over-estimate the input of marine SGD from ^{224}Ra, as we do not consider Ra inputs from

Table 4
Values used to calculate Ra-derived SGD fluxes into La Palme lagoon.

	General parameters			Units
A_{lagoon}	Surface of the lagoon	4.98		10^6 m^2
V_{bay}	Volume of the lagoon	3.98		10^6 m^3
	Ra terms	**^{223}Ra**	**^{224}Ra**	
C_{lagoon}	Average activity of the lagoon	7	119	dpm 100 L^{-1}
$C_{endmember}$	Activity of the endmember	17	527	dpm 100 L^{-1}
F_{diff}	Diffusive flux	1.1–1.7	32–53	dpm m^2 d^{-1}
	Ra flux			
J_{decay}	Flux associated with radioactive decay	0.17	9.2	10^8 dpm d^{-1}
J_{diff}	Diffusive flux in the lagoon	0.06–0.08	1.6–2.6	10^8 dpm d^{-1}
J_{SGD}	Flux associated with to SGD	0.09–0.11	6.5–7.6	10^8 dpm d^{-1}
	Water flow			
F_{SGD}	Submarine Groundwater Discharge	0.6–0.8	1.4–1.7	m^3 s^{-1}

bioirrigation and pore water exchange (Santos et al., 2012); we do not differentiate between these two processes. The flux derived from ^{223}Ra is in relative agreement with the one reported by Stieglitz et al. (2013) using a ^{222}Rn mass balance (0.29 m^3 s^{-1}). The higher flux derived from ^{224}Ra here may include inputs of ^{224}Ra from a shorter time-scale pore water exchange flux or inputs from bioirrigation, both of which are not explicitly taken into account in the mass balance. Regardless of the isotope, total SGD is greater than the water flux associated with the spring that discharges into the northern part of La Palme lagoon ($\leq$0.012 m^3 s^{-1}), suggesting that additional inputs of Ra associated with SGD take place in the lagoon. In particular, seawater recirculation may contribute significantly to the input of Ra into the lagoon, a pattern that was also observed with ^{222}Rn (Stieglitz et al., 2013).

4.3. Study of the coast-sea transfer offshore of the Calanque of Port-Miou

There is insufficient Ra data in Calanque of Port-Miou to achieve a Ra mass balance to estimate a SGD flux (Fig. 9). We can use the Ra activities to study the exchange rate between the Calanque and coastal seas. If the horizontal dispersion can be approximated by a diffusive process, a one-dimensional model can be written, assuming that advection is neglected and conditions are in steady-state (Moore, 2000):

$$\frac{dA}{dt} = K_h \frac{\partial^2 A}{\partial d^2} - \lambda A \tag{5}$$

Where A is the radium isotope activity; K_h is the eddy diffusion coefficient; d is the distance offshore; and λ the decay constant of the Ra isotope used. Assuming steady state, the solution of Eq. (5) is:

$$A_d = A_0 \exp\left(-d\sqrt{\frac{\lambda}{K_h}}\right) \tag{6}$$

Where A_d is the activity at the distance d from the coast and A_0 is the radium activity at the boundary (d = 0). The horizontal eddy coefficient (K_h) can thus be estimated from a plot ln(^{223}Ra) or ln(^{224}Ra) as a function of offshore distance (Moore, 2000; Fig. 11a, b, respectively). K_h is then defined as $K_h = \lambda/m^2$ where m is the slope of the linear regression.

Because several springs flow along the Calanque of Port-Miou, K_h was not calculated considering all the activities determined within the Calanque. We use samples CAL1, CAL2, CAL10, and CAL11 located at the mouth of the Calanque to estimate the horizontal eddy coefficient K_h, which thus quantifies mixing between the Calanque and offshore waters (Fig. 9). Using ^{223}Ra and ^{224}Ra, we obtain K_h values of 0.40 m^2 s^{-1} and 0.10 m^2 s^{-1}, respectively. Combining the K_h value to the ^{228}Ra gradient (Fig. 11c) allows us to calculate a flux of ^{228}Ra. We obtain a ^{228}Ra gradient of 990 dpm m^{-3} km^{-1}, which yields a ^{228}Ra flux of 3.4–6.8 *10^7 dpm d^{-1} per kilometer of coastline, considering 1.0–2.0 m as the thickness of waters impacted by the terrestrial groundwater input (Cockenpot, 2015). Considering that groundwater discharges only on the western side of the Calanque (i.e., 1.5 km) and using sample CAL7 as the endmember (i.e., spring in the northern part of the Calanque), we obtain a terrestrial groundwater flux of 0.6–1.2 m^3 s^{-1}. This value is slightly lower that the range of values reported earlier for that system by Arfib and Charlier (2016) who investigated the groundwater flux during 4 years between 2011 and 2015 (3–37 m^3 s^{-1}). Our estimate falls in the lower values because our study was conducted in July (dry season), in better agreement with the fluxes determined by Arfib and Charlier (2016) in July (3 m^3 s^{-1}). The SGD flux determined from our Ra isotope calculations require various assumptions, which include steady-state conditions, no water mass advection, assigning a value for the terrestrial groundwater endmember and neglecting vertical mixing. The difference between our estimated SGD flux to that of Arfib and Charlier (2016) may be due to these assumption. Conversely, this difference may reflect seasonality in response to seasonal precipitation.

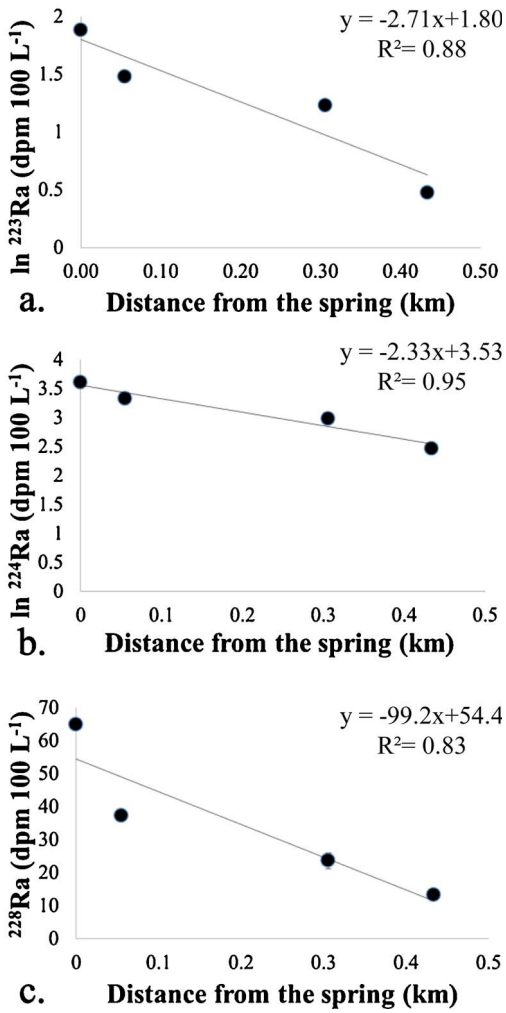

Fig. 11. Plots of a. ln(^{223}Ra), b. ln(^{224}Ra) and c. ^{228}Ra as a function of the distance offshore from the spring in Calanque of Port-Miou (CAL 10).

4.4. Estimation of terrestrial water fluxes from TIR images

Multiple temperature profiles were drawn across each TIR plume in a GIS (Figs. 2–4) in order to determine the boundary temperature between terrestrial SGD influenced pixels and ambient lagoon waters, from which the plumes two-dimensional surface area was calculated (Kelly et al., 2013; Tamborski et al., 2015). The boundary temperature is defined as the maximum change in pixel temperature, relative to pixel distance, averaged across the different temperature profiles. While the number of sites is limited, there appears to be a linear relationship between measured discharge rate and plume area for the lagoon seeps (Fig. 12). It should be noted that the TIR images here were not acquired during the same time period as the geochemical measurements. Additionally, the plume sizes will be strongly controlled by the prevailing wind speed and direction. Wind speeds were slightly higher during sampling in the field in April 2016 than during acquisition of the airborne TIR images. The relationship reported here between discharge rate and plume area is similar to observations along Hawaii (Kelly et al., 2013), Long Island Sound, NY (Tamborski et al., 2015) and Jeju Island, Korea (Lee et al., 2016). The regression equation slope of the lagoons (0.07 $m^3\ d^{-1}\ m^{-2}$) is similar to Port Jefferson Harbor, NY (0.1 $m^3\ d^{-1}\ m^{-2}$), a smaller embayment of the open Long Island Sound coastline (0.3 $m^3\ d^{-1}\ m^{-2}$; Tamborski et al., 2015). The relation between TIR area and SGD rates observed in our study is likely to differ from the open Mediterranean coastline, due to geomorphological and hydrogeochemical differences; therefore, we cannot extend this relation between TIR area and SGD flux to open sea coastlines (i.e. Fig. 5). As a result, we are unable to upscale our lagoon measurements to the Calanques de Marseille-Cassis. Conversely, the different regression slopes may describe differences between karst hydrogeology and the glacial till environment of Long Island, as well as the volcanic hydrogeology of Hawaii and Jeju Island. Mixing processes at the outlet of these systems may also be different from one location to the other. Nonetheless, these results suggest a robust relationship between thermal spatial characteristics and SGD.

This is the first SGD vs. TIR area relation developed for a karstic region, and suggests that this methodology is applicable in other karstic environments where prominent groundwater springs discharge at or near the surface. The estimation of terrestrial water

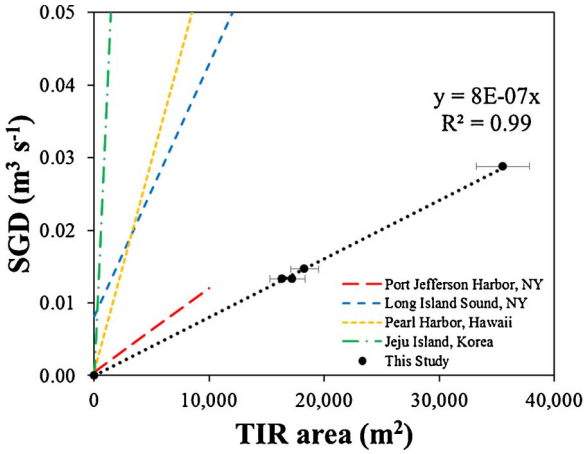

Fig. 12. Estimated SGD rates, calculated from radionuclide surveys, as a function of the TIR anomaly area. Data includes the La Palme lagoon spring (day and night; Fig. 2), Font Estramar spring (Fig. 3) and Salses-Leucate seep (Fig. 4). Port Jefferson Harbor, NY and Long Island Sound, NY slopes by Tamborski et al. (2015); Pearl Harbor, Hawaii slope by Kelly et al. (2013) and Jeju Island, Korea slope by Lee et al. (2016).

fluxes from TIR imagery requires ground-truthing data to validate the TIR anomalies, whether this is done *via* radionuclide tracers, salinity or manual flow measurements. However, this regression can be used to determine terrestrial water fluxes of other plumes from the lagoons investigated here. The application of a regression equation to upscale a TIR anomaly to an SGD flux is only applicable when the shoreline structure and aquifer properties are similar between the different study sites.

5. Conclusion

In this work, we report a new, unique dataset that covers the major sites of terrestrial groundwater discharge along the French Mediterranean coastline. To our knowledge, the airborne thermal infrared (TIR) images that we acquired to locate the different SGD sites constitutes the first case-study using this method along the French Mediterranean coastline. This method allowed us to observe the well-known karstic springs and also allowed us to detect new discharge locations at or near the seawater surface. Despite this success, the method was unable to capture deeper, well-known submerged springs (e.g. Vise spring in Thau lagoon which discharges at 30 m depth and is quickly mixed with the ambient water). Using salinity and Ra isotopes, we could characterize the different springs at their outlets. The use of Ra isotopes suggest that the transit time of groundwater-spring inputs to these coastal zones is on the order of one to several days along the French Mediterranean coastline. Ra isotope measurements indicate terrestrial groundwater discharge fluxes are less than 2% of the regional river discharge, while fluxes of marine groundwater (i.e. wind-driven seawater recirculation through the sediment) in La Palme lagoon are two orders of magnitude higher.

Conflict of intrerest

The authors declare no conflict of interests regarding the results from this work.
Simon Bejannin, Pieter van Beek, Thomas Stieglitz, Marc Souhaut and Joseph Tamborski.

Acknowledgements

We thank the three anonymous reviewers for their constructive comments on an earlier version of the paper that allowed us to significantly improve the quality of this manuscript. We thank European Union and Région Occitanie Pyrénées-Méditerranée for supporting the LAFARA underground laboratory through a FEDER funding (SELECT project). We are grateful to EDF (Electricité De France) for allowing us to run our germanium detectors in the tunnel of Ferrières. We thank Bruno Lansard for the help provided at the LAFARA underground laboratory of Ferrières. We thank Virginie Sanial for her participation to the survey that allowed us to acquire airborne TIR images. We thank Thierry Laugier (IFREMER Sète) and Pascal Brunet (HSM, Montpellier) who dived to collect the water samples at the outlet of the Vise spring (30 m depth). We thank Alexei Kouraev and Etienne Berthier at LEGOS for constructive discussions on TIR images. We are grateful to Kattalin Fortuné-Sans and Camille Pfleger (Parc Naturel Régional de la Narbonnaise en Méditerranée) and Laurence Fonbonne (Syndicat mixte RIVAGE Salses-Leucate). We thank Michel Bakalowicz (Hydrosciences Montpellier) and Perrine Fleury (BRGM Montpellier) who shared their knowledge prior to data collection. The project was funded by i) the 'Fondation de Coopération Scientifique Sciences et Technologies pour l'Aéronautique et l'Espace' through the program CYMENT (Cycle de l'eau et de la matière dans les bassins versants; PI: Anny Cazenave) for the field work conducted in 2009, ii) ANR-MED-SGD (ANR-15-CE01-0004; PI: Pieter van Beek) for the field work conducted in year 2016 and iii) CNES for funding the airborne TIR images acquired in 2012 as part of the Geomether project (PI: Pascal Allemand, Pieter van Beek being responsible for the acquisition of TIR images in that project). Thomas Stieglitz holds a chair @RAction of the French Agence National de Recherche ANR

(ANR-14-ACHN-0007-01, project medLOC), and is supported by the Labex OT-Med (ANR-11-LABEX-0061) funded by the "Investissements d'Avenir" program through the AMIDEX project (ANR-11- IDEX-0001-02). The phD thesis of Simon Bejannin and the postdoctoral fellowship of Joseph Tamborski are supported by FEDER funded by Europe and Région Occitanie Pyrénées-Méditerranée (SELECT project).

References

Aquilina, L., Ladouche, B., Doerfliger, N., Seidel, J.L., Bakalowicz, M., Dupuy, C., Le Strat, P., 2002. Origin, evolution and residence time of saline thermal fluids (Balaruc springs, southern France): implications for fluid transfer across the continental shelf. Chem. Geol. 192, 1–21. http://dx.doi.org/10.1016/S0009-2541(02)00160-2.

Arfib, B., Charlier, J.-B., 2016. Insights into saline intrusion and freshwater resources in coastal karstic aquifers using a lumped rainfall-discharge-salinity model (the Port-Miou brackish spring, SE France). J. Hydrol. 450, 148–161.

Arfib, B., Cavalera, T., Gilli, E., 2006. Influence de l'hydrodynamique sur l'intrusion saline en aquifère karstique côtier. C. R. Geosci. 338, 757–767. http://dx.doi.org/10.1016/j.crte.2006.07.001.

Beck, A.J., Rapaglia, J.P., Cochran, J.K., Bokuniewicz, H.J., Yang, S., 2008. Submarine groundwater discharge to great south bay, NY, estimated using Ra isotopes. Mar. Chem. 109, 279–291. http://dx.doi.org/10.1016/j.marchem.2007.07.011. Measurement of Radium and Actinium Isotopes in the marine environment.

Beusen, A.H.W., Slomp, C.P., Bouwman, A.F., 2013. Global land-ocean linkage: direct inputs of nitrogen to coastal waters via submarine groundwater discharge. Environ. Res. Lett. 8, 034035. http://dx.doi.org/10.1088/1748-9326/8/3/034035.

Bone, S.E., Charette, M.A., Lamborg, C.H., Gonneea, M.E., 2007. Has submarine groundwater discharge been overlooked as a source of mercury to coastal waters? Environ. Sci. Technol. 41, 3090–3095. http://dx.doi.org/10.1021/es0622453.

Burnett, W.C., Aggarwal, P.K., Aureli, A., Bokuniewicz, H., Cable, J.E., Charette, M.A., Kontar, E., Krupa, S., Kulkarni, K.M., Loveless, A., et al., 2006. Quantifying submarine groundwater discharge in the coastal zone via multiple methods. Sci. Total Environ. 367, 498–543.

Burnett, W.C., Wattayakorn, G., Taniguchi, M., Dulaiova, H., Sojisuporn, P., Rungsupa, S., Ishitobi, T., 2007. Groundwater-derived nutrient inputs to the Upper Gulf of Thailand. Cont. Shelf Res. 27, 176–190. http://dx.doi.org/10.1016/j.csr.2006.09.006.

COSOD II, 1987. Report of the Second Conference on Scientific Ocean Drilling.

Cavalera, T., 2007. Etude Du Fonctionnement Et Du Bassin d'alimentation De La Source Sous-marine De Port Miou (Cassis, Bouches-du-Rhône). Approche Multicritère (phdthesis). Université de Provence, Aix-Marseille I.

Charette, M.A., Buesseler, K.O., Andrews, J.E., 2001. Utility of radium isotopes for evaluating the input and transport of groundwater-derived nitrogen to a Cape Cod estuary. Limnol. Oceanogr. 46, 465–470. http://dx.doi.org/10.4319/lo.2001.46.2.0465.

Charette, M.A., Moore, W.S., Burnett, W.C., 2008. Uranium- and thorium-series nuclides as tracers of submarine groundwater discharge. In: Krishnaswami, S., Cochran, J.K. (Eds.), Radioactivity in the Environment. Elsevier, Oxford, UK. http://dx.doi.org/10.1016/S1569-4860(07)00005-8.

Cockenpot, S., 2015. Caractérisation des processus aux interfaces air-eau et sédiment-eau pour la quantification des apports d'eaux souterraines par le radium et le radon. Aix-Marseille.

Condomines, M., Gourdin, E., Gataniou, D., Seidel, J.-L., 2012. Geochemical behaviour of Radium isotopes and Radon in a coastal thermal system (Balaruc-les-Bains, South of France). Geochim. Cosmochim. Acta 98, 160–176. http://dx.doi.org/10.1016/j.gca.2012.09.010.

Elbaz-Poulichet, F., Seidel, J.-L., Othoniel, C., 2002. Occurrence of an anthropogenic gadolinium anomaly in river and coastal waters of Southern France. Water Res. 36, 1102–1105. http://dx.doi.org/10.1016/S0043-1354(01)00370-0.

Fleury, P., Bakalowicz, M., de Marsily, G., 2007. Submarine springs and coastal karst aquifers: a review. J. Hydrol. 339, 79–92. http://dx.doi.org/10.1016/j.jhydrol.2007.03.009.

Garcia-Solsona, E., Garcia-Orellana, J., Masqué, P., Dulaiova, H., 2008a. Uncertainties associated with 223Ra and 224Ra measurements in water via a Delayed Coincidence Counter (RaDeCC). Mar. Chem. 109, 198–219. http://dx.doi.org/10.1016/j.marchem.2007.11.006.

Garcia-Solsona, E., Masqué, P., Garcia-Orellana, J., Rapaglia, J., Beck, A.J., Cochran, J.K., Bokuniewicz, H.J., Zaggia, L., Collavini, F., 2008b. Estimating submarine groundwater discharge around Isola La Cura, northern Venice Lagoon (Italy), by using the radium quartet. Mar. Chem. 109, 292–306. http://dx.doi.org/10.1016/j.marchem.2008.02.007. Measurement of Radium and Actinium Isotopes in the marine environment.

Garcia-Solsona, E., Garcia-Orellana, J., Masqué, P., Rodellas, V., Mejías, M., Ballesteros, B., Domínguez, J.A., 2010. Groundwater and nutrient discharge through karstic coastal springs (Castello; Spain). Biogeosciences 7, 2625–2638. http://dx.doi.org/10.5194/bg-7-2625-2010.

Gilli, E., 2001. Compilation d'anciennes mesures de débit à port-Miou. apport à l'hydrogéologie de la basse provence. In: Presented at the 7th Conference on Limestone Hydrology and Fissured Media. Université de Franche Comté, Besançon, France.

Johannesson, K.H., Burdige, D.J., 2007. Balancing the global oceanic neodymium budget: evaluating the role of groundwater. Earth Planet. Sci. Lett. 253, 129–142. http://dx.doi.org/10.1016/j.epsl.2006.10.021.

Kelly, J.L., Glenn, C.R., Lucey, P.G., 2013. High-resolution aerial infrared mapping of groundwater discharge to the coastal ocean. Limnol. Oceanogr. Methods 11, 262–277.

Kwon, E.Y., Kim, G., Primeau, F., Moore, W.S., Cho, H.-M., DeVries, T., Sarmiento, J.L., Charette, M.A., Cho, Y.-K., 2014. Global estimate of submarine groundwater discharge based on an observationally constrained radium isotope model. Geophys. Res. Lett. 41, 8438–8444.

Lévêque, P.C., Gros, J.C., Sévérac, J., Siméon, C., Viguier, C., 1972. CRAS 274, 2841–2844.

Lee, Y.-W., Hwang, D.-W., Kim, G., Lee, W.-C., Oh, H.-T., 2009. Nutrient inputs from submarine groundwater discharge (SGD) in Masan Bay, an embayment surrounded by heavily industrialized cities, Korea. Sci. Total Environ. 407, 3181–3188. http://dx.doi.org/10.1016/j.scitotenv.2008.04.013. Human Impacts on Urban Subsurface Environments.

Lee, E., Kang, K., Hyun, S.P., Lee, K.-Y., Yoon, H., Kim, S.H., Kim, Y., Xu, Z., Kim, D., Koh, D.-C., Ha, K., 2016. Submarine groundwater discharge revealed by aerial thermal infrared imagery: a case study on Jeju Island, Korea. Hydrol. Processes 30, 3494–3506. http://dx.doi.org/10.1002/hyp.10868.

Ludwig, W., Dumont, E., Meybeck, M., Heussner, S., 2009. River discharges of water and nutrients to the Mediterranean and Black Sea: major drivers for ecosystem changes during past and future decades? Prog. Oceanogr. 80, 199–217. http://dx.doi.org/10.1016/j.pocean.2009.02.001.

Mejías, M., Ballesteros, B.J., Antón-Pacheco, C., Domínguez, J.A., Garcia-Orellana, J., Garcia-Solsona, E., Masqué, P., 2012. Methodological study of submarine groundwater discharge from a karstic aquifer in the Western Mediterranean Sea. J. Hydrol. 464–465, 27–40. http://dx.doi.org/10.1016/j.jhydrol.2012.06.020.

Moore, W.S., Arnold, R., 1996. Measurement of 223Ra and 224Ra on coastal waters using a delayed coincidence counter. J. Geophys. Res. Oceans 101, 1321–1329. http://dx.doi.org/10.1029/95JC03139.

Moore, W.S., Reid, D.F., 1973. Extraction of radium from natural waters using manganese-impregnated acrylic fibers. J. Geophys. Res. 78, 8880–8886. http://dx.doi.org/10.1029/JC078i036p08880.

Moore, W.S., 1996. Using the radium quartet for evaluating groundwater input and water exchange in salt marshes. Geochim. Cosmochim. Acta 60, 4645–4652. http://dx.doi.org/10.1016/S0016-7037(96)00289-X.

Moore, W.S., 1999. The subterranean estuary: a reaction zone of ground water and sea water. Mar. Chem. 65, 111–125. http://dx.doi.org/10.1016/S0304-4203(99)00014-6.

Moore, W.S., 2000. Ages of continental shelf waters determined from 223Ra and 224Ra. J. Geophys. Res. Oceans 105, 22117–22122. http://dx.doi.org/10.1029/1999JC000289.

Moore, W.S., 2006. Radium isotopes as tracers of submarine groundwater discharge in Sicily. Cont. Shelf Res. 26, 852–861. http://dx.doi.org/10.1016/j.csr.2005.12.004.

Moore, W.S., 2008. Fifteen years experience in measuring 224Ra and 223Ra by delayed-coincidence counting. Mar. Chem. 109, 188–197. http://dx.doi.org/10.1016/j.

marchem.2007.06.015.
Mulligan, A.E., Charette, M.A., 2009. Groundwater flow to the coastal ocean. In: John, H.S., Karl, K.T., Steve, A.T. (Eds.), Encyclopedia Ocean Science. Academic, Oxford, pp. 88–97.
Muricy, G., 1991. Structure des peuplements de spongiaires autour de l'égout de Cortiou (Marseille, France). Vie Milieu 41, 205–221.
Ollivier, P., Claude, C., Radakovitch, O., Hamelin, B., 2008. TIMS measurements of 226Ra and 228Ra in the Gulf of Lion, an attempt to quantify submarine groundwater discharge. Mar. Chem. 109, 337–354. http://dx.doi.org/10.1016/j.marchem.2007.08.006. Measurement of Radium and Actinium Isotopes in the marine environment.
Peterson, R.N., Burnett, W.C., Taniguchi, M., Chen, J., Santos, I.R., Ishitobi, T., 2008. Radon and radium isotope assessment of submarine groundwater discharge in the Yellow River delta, China. J. Geophys. Res. Oceans 113, C09021. http://dx.doi.org/10.1029/2008JC004776.
Rodellas, V., Garcia-Orellana, J., Masqué, P., Feldman, M., Weinstein, Y., 2015. Submarine groundwater discharge as a major source of nutrients to the Mediterranean Sea. Proc. Natl. Acad. Sci. 112, 3926–3930.
Santos, I.R., Eyre, B.D., Huettel, M., 2012. The driving forces of porewater and groundwater flow in permeable coastal sediments: a review. Estuar. Coast. Mar. Sci. 98, 1–15. http://dx.doi.org/10.1016/j.ecss.2011.10.024.
Sawyer, A.H., David, C.H., Famiglietti, J.S., 2016. Continental patterns of submarine groundwater discharge reveal coastal vulnerabilities. Science 353, 705–707. http://dx.doi.org/10.1126/science.aag1058.
Schubert, M., Scholten, J., Schmidt, A., Comanducci, J.F., Pham, M.K., Mallast, U., Knoeller, K., 2014. Submarine Groundwater Discharge at a single spot location: evaluation of different detection approach. Water 6 (3), 584–601. http://dx.doi.org/10.3390/w6030584.
Serrat, P., 1999. Dynamique sédimentaire actuelle d'un système fluvial méditerranéen: l'Agly (France): present sediment yield from a Mediterranean fluvial system: the Agly river (France). C. R. Acad. Sci.-Ser. IIA-Earth Planet. Sci. 329, 189–196.
Slomp, C.P., Van Cappellen, P., 2004. Nutrient inputs to the coastal ocean through submarine groundwater discharge: controls and potential impact. J. Hydrol. 295, 64–86. http://dx.doi.org/10.1016/j.jhydrol.2004.02.018.
Stieglitz, T.C., van Beek, P., Souhaut, M., Cook, P.G., 2013. Karstic groundwater discharge and seawater recirculation through sediments in shallow coastal Mediterranean lagoons, determined from water, salt and radon budgets. Mar. Chem. 156, 73–84. http://dx.doi.org/10.1016/j.marchem.2013.05.005. Radium and Radon Tracers in Aquatic Systems.
Stieglitz, T., 2005. Submarine groundwater discharge into the near-shore zone of the Great Barrier Reef, Australia. Mar. Pollut. Bull. 51, 51–59. http://dx.doi.org/10.1016/j.marpolbul.2004.10.055. Catchment to Reef: Water Quality Issues in the Great Barrier Reef Region.
Sun, Y., Torgersen, T., 1998. The effecys of water content and Mn-fiber surface conditions on 224Ra measurement by 220Rn emanation. Mar. Chem. 62, 299–306.
Swarzenski, P.W., 2007. U/Th series radionuclides as coastal groundwater tracers. Chem. Rev. 107, 663–764. http://dx.doi.org/10.1021/cr0503761Tamborski.
Tamborski, J.J., Rogers, A.D., Bokuniewicz, H.J., Cochran, J.K., Young, C.R., 2015. Identification and quantification of diffuse fresh submarine groundwater discharge via airborne thermal infrared remote sensing. Remote Sens. Environ. 171, 202–217. http://dx.doi.org/10.1016/j.rse.2015.10.010.
Taniguchi, M., Burnett, W.C., Cable, J.E., Turner, J.V., 2002. Investigation of submarine groundwater discharge. Hydrol. Process. 16, 2115–2129. http://dx.doi.org/10.1002/hyp.1145.
Trezzi, G., Garcia-Orellana, J., Santos-Echeandia, J., Rodellas, V., Garcia-Solsona, E., Garcia-Fernandez, G., Masqué, P., 2016. The influence of a metal-enriched mining waste deposit on submarine groundwater discharge to the coastal sea. Mar. Chem. 178, 35–45.
Wilke, M., Boutiere, H., 2000. Hydrobiological, physical and chemical characteristics and spatio-temporal dynamics of an oligotrophic Mediterranean lagoon: the Etang de La Palme (France). Vie Milieu 50, 101–115.
Wilson, J., Rocha, C., 2012. Regional scale assessment of Submarine Groundwater Discharge in Ireland combining medium resolution satellite imagery and geochemical tracing techniques. Remote Sens. Environ. 119, 21–34.
van Beek, P., Souhaut, M., Reyss, J.-L., 2010. Measuring the radium quartet (228Ra, 226Ra, 224Ra, 223Ra) in seawater samples using gamma spectrometry. J. Environ. Radioact. 101, 521–529. http://dx.doi.org/10.1016/j.jenvrad.2009.12.002. Radium and Radon Isotopes as Environmental Tracers.
van Beek, P., Souhaut, M., Lansard, B., Bourquin, M., Reyss, J.-L., von Ballmoos, P., Jean, P., 2013. LAFARA: a new underground laboratory in the French Pyrénées for ultra low-level gamma-ray spectrometry. J. Environ. Radioact. 116, 152–158. http://dx.doi.org/10.1016/j.jenvrad.2012.10.002.